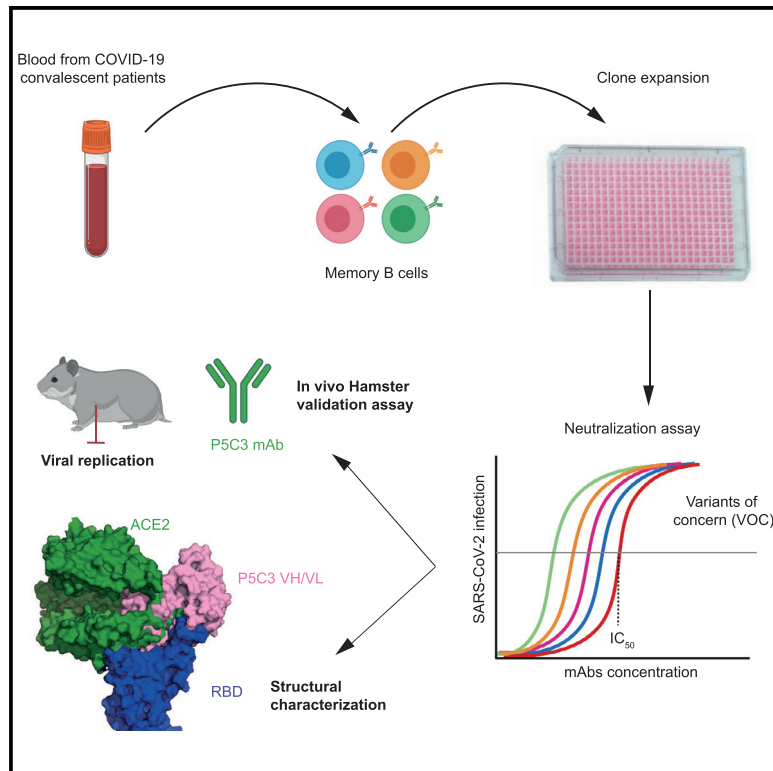# Cell Reports

A highly potent antibody effective against SARS-CoV-2 variants of concern

Graphical abstract

Authors

Craig Fenwick, Priscilla Turelli, Laurent Perez, ..., Yves Lévy, Didier Trono, Giuseppe Pantaleo

Correspondence

didier.trono@epfl.ch (D.T.),
giuseppe.pantaleo@chuv.ch (G.P.)

In brief

Fenwick et al. identify a highly potent anti-SAR-CoV-2 antibody that retains full activity against all variants of concern, demonstrates *in vivo* prophylactic protection in a hamster challenge model, and could be used prophylactically, as it has an extended *in vivo* half-life.

Highlights

- Highly potent anti-SARS-CoV-2 antibody has broad activity against all VOCs

- Binding epitope strongly overlaps with the RBD surface necessary for ACE2 interaction

- Complete prophylactic protection in the SARS-CoV-2-infected hamster challenge model

- The anti-SARS-CoV-2 antibody could be used in a prophylactic setting

CellPress

Article

A highly potent antibody effective against SARS-CoV-2 variants of concern

Craig Fenwick,[1,12] Priscilla Turelli,[2,12] Laurent Perez,[1,12] Céline Pellaton,[1] Line Esteves-Leuenberger,[1] Alex Farina,[1] Jérémy Campos,[1] Erica Lana,[1] Flurin Fiscalini,[1] Charlène Raclot,[2] Florence Pojer,[2] Kelvin Lau,[2] Davide Demurtas,[2] Marc Descatoire,[1] Victor S. Joo,[1] Mathilde Foglierini,[1] Alessandra Noto,[1] Rana Abdelnabi,[3] Caroline S. Foo,[3] Laura Vangeel,[3] Johan Neyts,[3] Wenjuan Du,[4] Berend-Jan Bosch,[4] Geertruida Veldman,[5] Pieter Leyssen,[3] Volker Thiel,[6] Roger LeGrand,[7] Yves Lévy,[8,9,10] Didier Trono,[2,*] and Giuseppe Pantaleo[1,8,11,13,*]

[1]Service of Immunology and Allergy, Department of Medicine, Lausanne University Hospital and University of Lausanne, Lausanne, Switzerland
[2]School of Life Sciences, Ecole Polytechnique Fédérale de Lausanne, Lausanne, Switzerland
[3]KU Leuven Department of Microbiology, Immunology and Transplantation, Rega Institute for Medical Research, Laboratory of Virology and Chemotherapy, 3000 Leuven, Belgium
[4]Virology Section, Infectious Diseases and Immunology Division, Department of Biomolecular Health Sciences, Faculty of Veterinary Medicine, Utrecht University, Utrecht, the Netherlands
[5]Abbvie Bioresearch Center, Worcester, MA, USA
[6]Department of Infectious Diseases and Pathobiology, Vetsuisse Faculty, University of Bern, Bern, Switzerland
[7]CEA, Université Paris Sud 11, INSERM U1184, Center for Immunology of Viral Infections and Autoimmune Diseases, IDMIT Department, IBFJ, Fontenay-aux-Roses, France
[8]VRI, Université Paris-Est Créteil, Faculté de Médecine, INSERM U955, 94010 Créteil, France
[9]INSERM U955, Equipe 16, Creteil, France
[10]AP-HP, Ho^pital Henri-Mondor Albert-Chenevier, Service d'Immunologie Clinique et Maladies Infectieuses, Creteil, France
[11]Swiss Vaccine Research Institute, Lausanne University Hospital and University of Lausanne, Switzerland
[12]These authors contributed equally
[13]Lead contact
*Correspondence: didier.trono@epfl.ch (D.T.), giuseppe.pantaleo@chuv.ch (G.P.)
https://doi.org/10.1016/j.celrep.2021.109814

SUMMARY

Control of the ongoing SARS-CoV-2 pandemic is endangered by the emergence of viral variants with increased transmission efficiency, resistance to marketed therapeutic antibodies, and reduced sensitivity to vaccine-induced immunity. Here, we screen B cells from COVID-19 donors and identify P5C3, a highly potent and broadly neutralizing monoclonal antibody with picomolar neutralizing activity against all SARS-CoV-2 variants of concern (VOCs) identified to date. Structural characterization of P5C3 Fab in complex with the spike demonstrates a neutralizing activity defined by a large buried surface area, highly overlapping with the receptor-binding domain (RBD) surface necessary for ACE2 interaction. We further demonstrate that P5C3 shows complete prophylactic protection in the SARS-CoV-2-infected hamster challenge model. These results indicate that P5C3 opens exciting perspectives either as a prophylactic agent in immunocompromised individuals with poor response to vaccination or as combination therapy in SARS-CoV-2-infected individuals.

INTRODUCTION

Since emerging in the Hubei province of China in late 2019, the severe acute respiratory syndrome coronavirus 2 (SARS-CoV-2) has provoked a global health crisis. The ongoing pandemic has resulted in more than 3 million deaths, a near collapse of health care networks, and has had a devastating impact on societies and economies around the world (Abrams and Szefler, 2020; Zhou et al., 2020). Apart from the COVID-19 disease associated with infection, 5%–10% of symptomatic individuals, including young adults, have longer-term health consequences of SARS-CoV-2 infection (Sudre et al., 2021).

The rapid response of scientific communities around the world has led to unparalleled progress in SARS-CoV-2 viral diagnostics and COVID-19 immune monitoring, the delineation of risk factors for serious disease, the development of protective vaccines, and the identification of some treatment options, including monoclonal antibodies with antiviral neutralizing properties. Despite these successes, the worldwide propagation of SARS-CoV-2 has resulted in the rapid evolution of this virus, with the emergence of variants of concern (VOCs) that erode these hard-fought advances. The B.1.1.7 variant (also called 501Y.V1) first identified in the UK contains mutations that augment virus transmission rates by 65%–74% (Davies et al.,

2021; Volz et al., 2021), launching in late 2020 a wave of infections that rapidly spread in many regions of the world. The B.1.351 variant (a.k.a. 501Y.V2) identified soon after in South Africa and the closely related P.1 (a.k.a. 501Y.V3, B.1.1.28 or Brazilian VOC) carry many of the same changes, including a triple substitution in the ACE2 receptor-binding domain (RBD) of the viral Spike protein. These mutations, most notably at positions 417, 484, and 501 of Spike, result in increased affinity of the virus for the ACE2 cell surface receptor and/or in reduced recognition by neutralizing antibodies, most of which recognize the RBD (Barnes et al., 2020; Korber et al., 2020; Ozono et al., 2021; Piccoli et al., 2020). As a result, these VOCs have been found largely to escape immunity induced by some COVID-19 vaccines and have resulted in a resurgence of infection in several regions of the world, with many documented cases of re-infection (Wang et al., 2021b; Zhou et al., 2021). Furthermore, these VOCs have a significant impact on the efficacy of neutralizing antibodies developed as therapeutic agents for SARS-CoV-2-infected individuals (Baum et al., 2020; Wang et al., 2021b).

The large-scale rollout of COVID-19 vaccines is anticipated to mitigate the consequences of SARS-CoV-2 exposure for most people. However, it will not improve the situation of the numerous individuals unable to mount an effective humoral immune response following vaccination due either to some form of immunodeficiency or to immunosuppression following organ transplant or as part of the treatment of immune diseases or some cancers, notably by B cell depletion. Potent and broadly active SARS-CoV-2 monoclonal antibodies, so far considered essentially for their therapeutic potential in severely ill COVID-19 patients, could also address this important unmet clinical need as agents of passive immunization against the virus.

RESULTS

Identification of P5C3, a highly potent SARS-CoV-2 neutralizing antibody

In the present study, we screened a cohort of 40 hospitalized COVID-19 patients for the presence of anti-Spike antibodies between 7 and 30 days after symptoms onset. At ~3 months post-infection, we obtained blood samples from eight of these subjects presenting the highest levels of anti-Spike immunoglobulin (Ig)G antibodies. Plasmablasts ($CD19^+/IgM^-/IgD^-/CD27^+/CD38^{hi}$) and memory B cells ($CD19^+/IgM^-/IgD^-/CD27^+$) recognized by fluorescently labeled Spike ectodomain and RBD were sorted and a total of 1,165 B cell clones from the eight donors (n = 41–239 by donor) produced anti-Spike binding antibodies. We selected 103 clones (n = 6–15 by donor) with the highest Spike binding activity for monoclonal antibody (mAb) production via expression of paired heavy and light chains in Chinese hamster ovary (CHO) cells. The 10 purified mAbs with the strongest affinity to the 2019-nCoV Spike trimer (half-maximal effective concentration [EC_{50}] values of 0.012–0.120 μg/mL) were kept for further characterization (Figure S1A).

Given that emerging VOCs contain mutations in and around the Spike RBD that confer resistance to potent neutralizing mAbs (Korber et al., 2020; Ozono et al., 2021), we next examined the binding properties of our 10 prioritized mAbs to Spike derivatives with mutations and/or deletions found in VOCs.

REGN1033, REGN10987, and S309, three mAbs used in the clinic, were tested in parallel as benchmarks (Figures 1A and S1B). In binding studies with different Spike protein mutations, including N439K, S477N, E484K (present in B.1.351, P.1, and B1.526/B1.232 New York variants), L452R (present in the Californian CAL.20C variant) and full B.1.1.7, B.1.351, and P.1 variants (Table S1), P5C3 exhibited the highest affinity and without a significant loss in binding for any of the tested Spike variants (EC_{80} values of 0.02–0.035 μg/mL). In contrast, REGN10933 exhibited a 60-fold, 15-fold, and 195-fold reduced binding affinity for the K417N/E484K/N501Y, B.1.351, and P.1 Spike variants, respectively. While REGN10987 was comparatively less affected with these variants, it displayed a 4.4-fold reduced binding affinity to the Spike N439K mutation (Figure 1A). S309 bound similarly to all tested Spike versions, but its affinity was on average 12-fold reduced compared with P5C3 (EC_{80} of 0.23–0.50 μg/mL). As our nine other preselected mAbs presented various degrees of reduced affinity to Spike variants (Figure S1B), P5C3 was prioritized for further characterization and development.

As a first step, competitive Spike binding studies were performed with the ACE2 protein and therapeutic antibodies known to recognize distinct epitopes on the RBD. P5C3 competed for RBD binding with ACE2 and REGN10933 but had a non-competitive binding profile (<20% blocking) with REGN10987 or S309 mAbs (Figure 1B). Of note, this analysis additionally revealed that through stearic hindrance or binding-induced conformational change in RBD, REGN10987 is at least partially competitive with both REGN10933 and S309 mAbs for RBD binding.

We then measured the ability of P5C3 and benchmark mAbs to neutralize 2019-nCOV SARS-CoV-2 and VOCs using assays based on the infection of ACE2-positive cells with either lentiviral particles pseudotyped with Spike or for infectious SARS-CoV-2 strains with sequence variants in the Spike gene.

P5C3 had the most potent neutralizing activity against 2019-nCoV Spike-coated pseudoviruses, with an EC_{80} value of 0.021 μg/mL (Figures 2A and 2B). It displayed equally strong neutralization of all tested Spike mutations, including the E484K substitution that is a key mutation found in B.1.351, P.1, and the new B1.526 variant identified in New York. The sole exception was the S477N mutant for which the EC_{80} of P5C3 increased modestly to 0.08 μg/mL. REGN10933 was only ~2-fold less active than P5C3 at blocking the original 2019-nCoV, but consistent with published results (Baum et al., 2020; Wang et al., 2021b) it had a significant loss in neutralizing activity against pseudoviruses produced with the Spike E484K mutation (EC_{80} of 0.325 μg/mL for E484K/N501Y and 5.72 μg/mL for K417N/E484K/N501Y) present in both B1.351, P.1, and B1.526 VOCs. REGN10987 was a few fold less potent than P5C3 against most Spike mutations tested, notably those harboring the E484K mutation (7- to 11-fold), and it was further considered as inactive against particles coated with N439K Spike (EC_{80} of 3.73 μg/mL) as previously described (Thomson et al., 2021).

Pseudoviral assays are valuable tools for profiling the impact on neutralization of large series of Spike mutations. However, neutralization studies using the real SARS-CoV-2 virus are essential given that some classes of mAbs, including S309, operate by mechanisms distinct from direct Spike/ACE2 blockade and may demonstrate incomplete neutralization in pseudotype
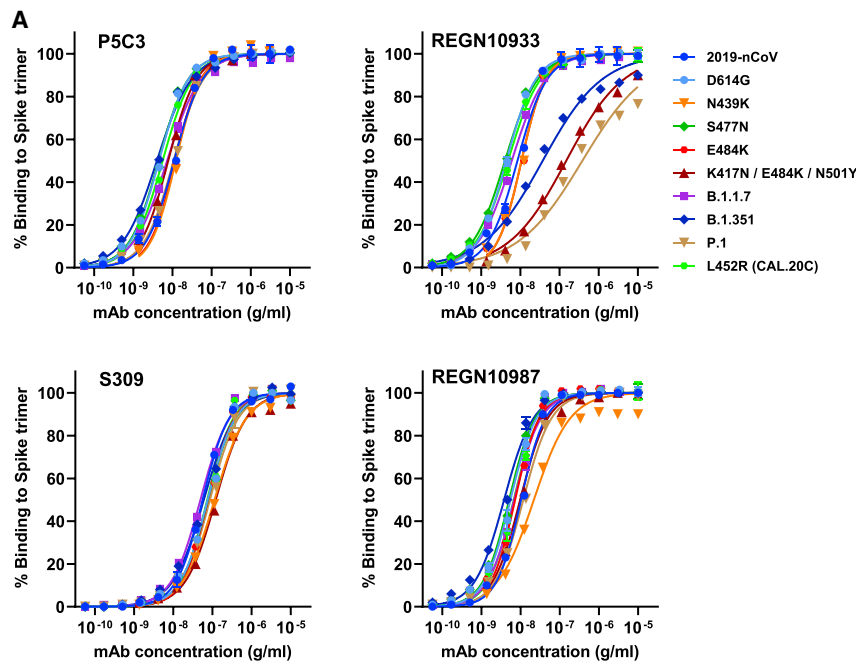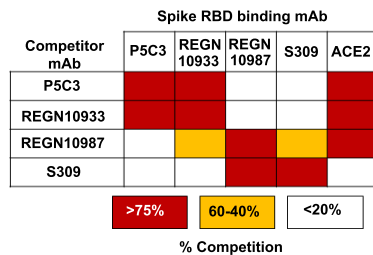
Figure 1. Identification of P5C3, a human mAb with high affinity binding to trimeric spike protein with mutations found in VOCs

(A) Binding of P5C3 and three benchmark anti-SARS-CoV-2 therapeutic mAbs to 10 trimeric Spike proteins produced with mutations found in VOCs. Representative of two to four independent experiments with each concentration response tested in duplicate. Mean values ± SEM are shown.

(B) Competitive binding studies between antibodies binding to the Spike RBD protein. RBC-coupled beads pre-incubated with saturating concentrations of competitor antibody were used for binding studies with mAbs or ACE2. Competitors induced either strong blocking (red boxes), partial competition (orange boxes), or non-competitive (white boxes) binding with the corresponding mAb to RBD.

tency against the D614G and B.1.1.7 variant viruses but REGN10933 lost significant potency against both the B.1.351 and mink-related variants (Figure 3A) (Baum et al., 2020; Wang et al., 2021b). REGN10987 and S309 both displayed broad neutralization potential against these variants, but EC$_{80}$ values of REGN10987 were 5.6- to 9.5-fold less potent than measured for P5C3 LS against the 2019-nCoV and D614G viruses, and S309 was 28- to 177-fold less potent against all tested viruses (Figure 3B).
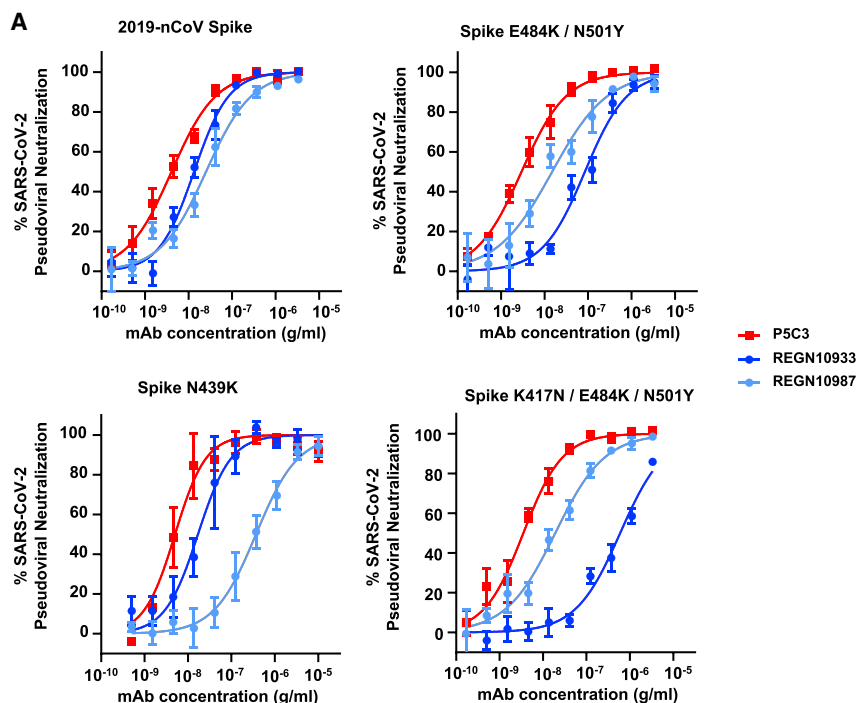
Thus, the combination of binding studies with neutralization assays performed with pseudotyped- or live virus-based assays singled out P5C3 as a mAb with unmatched potency against the broad range of Spike mutations found in circulating VOCs, prompting us to perform additional studies aimed at characterizing how it interacts with its antigenic target.

assays (Rappazzo et al., 2020). Therefore, we tested P5C3 and the benchmark therapeutic mAbs against different SARS-CoV-2 variants in live virus cytopathic effect assays. Viruses included, in addition to the 2019-nCoV strain, the D614G Spike mutant that emerged early in the pandemics, the B.1.1.7 and B.1.351 VOCs, and a recent variant found in a mink-related cluster, with documented back-transmission to humans (Hoffmann et al., 2021). We also used in these experiments a modified form of P5C3 containing the so-called LS mutation in the Fc domain (M428L/N434S), previously demonstrated to confer an extended half-life in vivo (Zalevsky et al., 2010; Gautam et al., 2016). This effect, important for envisioning the prophylactic use of P5C3, was verified in the human FcRn transgenic mouse model, where it exhibited a 2.4-fold increased half-life compared to its unmodified P5C3 IgG1 counterpart (Figure S2).

P5C3 LS demonstrated the most potent neutralizing activity of all mAbs tested with EC$_{80}$ values of 0.011, 0.022, 0.011, 0.014, and 0.008 µg/mL against the 2019-nCoV strain, the D614G mutation, B.1.1.7, B.1.351, and mink variant viruses, respectively (EC$_{80}$ values ranging from 50 to 140 pM). Neutralization profiles of reference therapeutic mAbs were consistent with previous publications where REGN10933, REGN10987, and S309 maintained po-

Structural basis for tight binding and potency against VOCs

To understand the structural basis of P5C3 potent neutralization of SARS-CoV-2 VOCs, we characterized the complex formed by the stabilized SARS-CoV-2 Spike trimer, containing the D614G mutation in the ectodomain backbone (Walls et al., 2020; Wrapp et al., 2020a) and P5C3 Fab fragments using single particle cryoelectron microscopy (cryo-EM) at a resolution of 3.5 Å (Figures 4A and 4B; Table S2; Figures S3 and S4). The EM map was generated by performing non-uniform refinement (Figure S3) followed by local refinement of the Fab-RBD interacting region to reach 4.3 Å of local resolution (Figure S4), with the Fab bound to the RBD in the open conformation of Spike (Figures 4A–4C). Next, we built an atomic model for the quaternary structure of the complex by positioning the Cα chains and side chains of the amino acids when they were visible, for the Fab and Spike (Figures 4C and S4).

First, we characterized the overall interaction between the P5C3 paratope and the viral Spike trimer. We confirmed that its target

A

2019-nCoV Spike

Spike E484K / N501Y

Spike N439K

Spike K417N / E484K / N501Y

■ P5C3
● REGN10933
● REGN10987

B

Spike PV assay	P5C3		REGN10933		REGN10987	
	EC$_{50}$	EC$_{80}$	EC$_{50}$	EC$_{80}$	EC$_{50}$	EC$_{80}$
2019-nCoV	0.004	0.021	0.014	0.047	0.025	0.134
D614G	0.014	0.042	0.037	0.143	0.041	0.233
A222V	0.003	0.021	0.015	0.057	0.016	0.070
N439K	0.014	0.029	0.037	0.086	0.697	3.730
S477N	0.035	0.080	0.048	0.144	0.045	0.140
Q493K	0.010	0.034	0.033	0.108	0.037	0.187
S494P	0.006	0.025	0.028	0.098	0.043	0.245
E484K/N501Y	0.004	0.021	0.084	0.325	0.039	0.254
K417N/E484K/N501Y	0.013	0.029	0.925	5.720	0.033	0.210

<0.05	0.05 – 0.25	0.25 – 1.0	>1

EC$_{50}$ / EC$_{80}$ values (µg/ml)

Figure 2. P5C3 demonstrates potent and broad neutralizing activity against spike-coated pseudoviruses

(A) Neutralization of lentiviral particles pseudotyped with SARS-CoV-2 Spike expressing variants of concern in a 293T-ACE2 infection assay. All Spike proteins with mutations except Q493K and S494P contained the D614G substitution that became dominant early in the pandemic. Results shown are the average of two independent experiments with each concentration response tested in triplicate. Mean values ± SEM are shown.

(B) Heatmap showing EC$_{50}$ and EC$_{80}$ neutralization potencies for the indicated mAbs. Results are the average of two to four independent experiments with each concentration response tested in duplicates or triplicates.

on the Spike surface (Figures S4E and S5C). In the CDR H3, P95, G100, S100a, C100b, D100d, and F100f make multiple contacts with the RBD thumb region (residues 475–489; Figures S4E and S5D), while in CDR H2, W50 and S54 provide additional interactions at the paratope-epitope interface (Figures S4E, S5C, and S5D). Moreover, CDRs at the interface are in close proximity to form hydrophobic interactions and aromatic contacts with residues F456, Y473, F486, and Y489 of Spike. This binding mode is unusual for paratope-epitope interactions owing to the broad spatial separation of CDRH3 and CDRL3 (Figures 4D, S5C, and S5D). Interestingly, the mAb binding epitope also partially covers the antiparallel β5, β6 strands of Spike (residues 451–456 and 491–495), a domain that should not be subjected to the development of resistance mutations owing to its essential folding function (Figure S5B).

epitope overlaps with the ACE2 receptor-binding site of Spike (Figure 4D), indicating that P5C3 is a class I neutralizing antibody, that is, ACE2 blocking, by binding RBD in the open only conformation (Barnes et al., 2020). Upon analysis of the paratope/epitope interaction, we discovered that the P5C3-Spike interface covers a large region of about 600 Å² surface centered on F486 (Figures 4D, S4D, S4E, and S5A) and involving 23 aa of P5C3 and 21 aa of the Spike RBD (Figures 4D, S5C, and S5D). This result is consistent with the strong measured affinity and potency of the mAb. Moreover, we could determine that P5C3 binds its epitope through five of its complementarity-determining regions (CDRs), namely CDRs H1, H2, and H3 of the heavy chain and L1 and L3 of the light chain (Figures 4D, S5C, and S5D). Interestingly, we observed that CDR H3 is stabilized by an intra-loop disulfide bond between C97 and C100b (Kabat numbering) that restrains the loop in an optimal binding conformation (Figures S4E and S5B). Analysis of the CDR loop contacts revealed that for the light chain CDRs, Y32 in L1 and W96 in L3 are in close contact with P479 and F486, respectively,

To understand further why P5C3 binding is not affected by mutations harbored by SARS-CoV-2 variants, we superimposed our structure with that solved of the ACE2-RBD interaction (PDB: 6M0J) (Lan et al., 2020) (Figures 5A and 5B). ACE2 covers around 860 Å² on the RBD, compared with 600 Å² for P5C3 where P5C3 interacts with the RBD ridge at a 90° angle compared with a 130° angle for ACE2 (Wang et al., 2020b) (Figures 5A and 5B). Importantly, ~70% (414 Å² out of 600 Å²) of the P5C3 buried surface area is shared with the ACE2 site on the RBD. P5C3 and ACE2 binding overlaps with L455, F456, A475, G476, S477, E484, F486, N487, Y489 and Q493 of the RBD, which constitute a core for tight binding. Indeed, these residues form a hydrophobic patch surrounding F486 on the RBD, where F486 interacts with Q24, L79, M82, and Y83 of ACE2. Furthermore, additional critical residues necessary for RBD interaction with ACE2 are blocked by P5C3, such as F456 and Q493 (Lan et al., 2020) (Figure S5D).

We went on to compare the P5C3 binding mode to that of leader ACE2 blocking mAb candidates currently in clinical trials
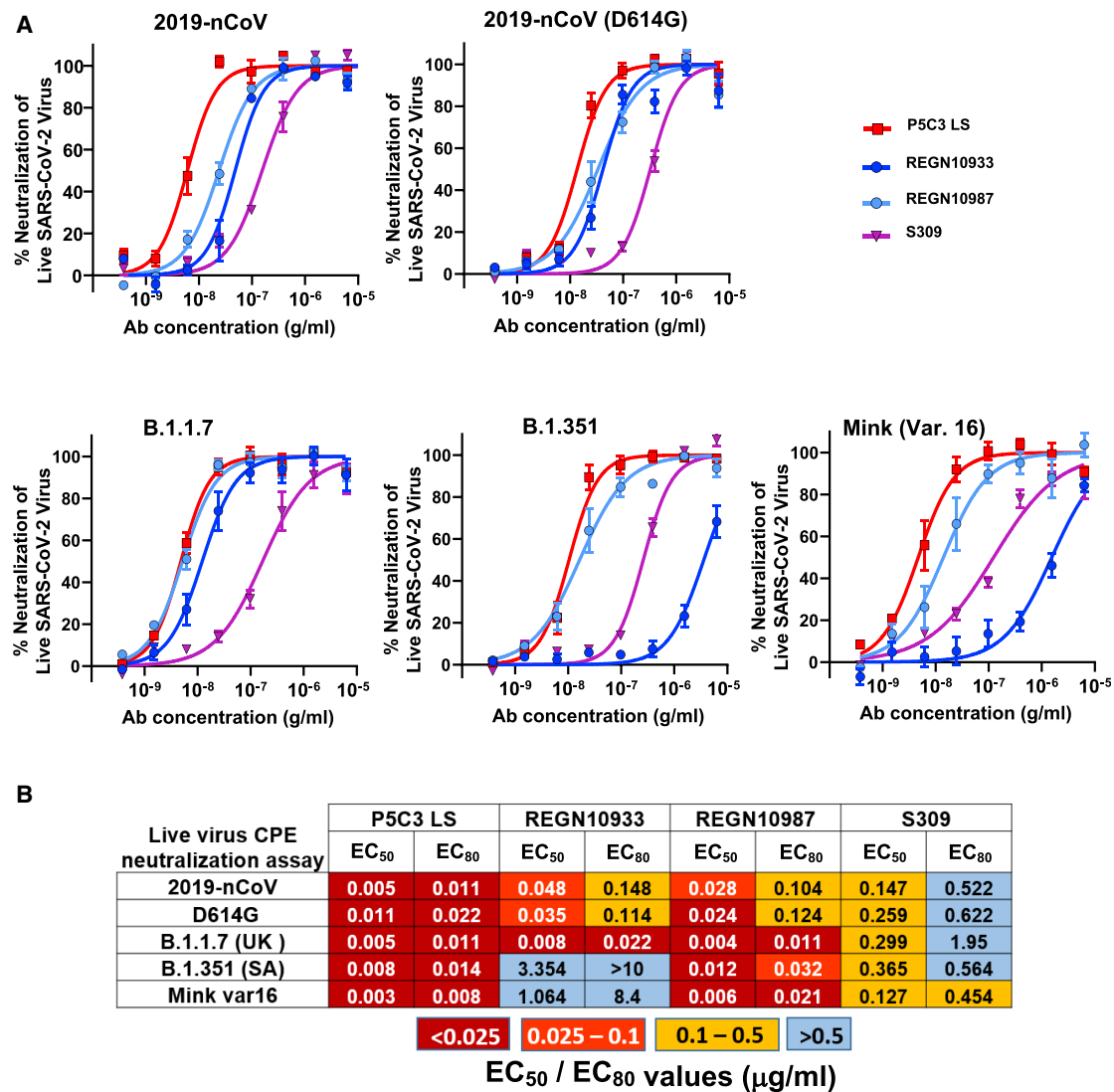
Figure 3. P5C3 LS demonstrates potent neutralizing activity against SARS-CoV-2 VOCs

(A) Neutralization activity of mAbs performed in a live SARS-CoV-2 infectious virus cytopathic effect assay. The indicated SARS-CoV-2 variants were used to infect Vero E6 *in vitro* in the absence and presence of concentration response of the indicated mAb evaluated in duplicates or triplicates.

(B) Heatmap showing EC_{50} and EC_{80} neutralization potencies for the mAbs indicated in pseudoviral assay produced using the indicated mutated version of Spike. Results shown are the average of two to four independent experiments with each concentration response tested in duplicates or triplicates. Mean values ± SEM are shown.

for REGN10933, REGN10987 (PDB: 6XDG) (Hansen et al., 2020a), and LY-CoV016 (PDB: 7C01) (Shi et al., 2020) (Figure 5C). It was recently demonstrated that the neutralizing activity of these three mAbs could be negatively affected by mutation identified in circulating variants that are not affecting ACE2 binding to the open RBD (Starr et al., 2021) (Figure 5D). In particular, mutations K417T/N, N439K, S477N, E484K, and N501Y have been reported to increase their affinity to ACE2 and/or render the mAbs LY-CoV555 (Jones et al., 2020), REGN10933, and REGN10987 less efficient (Baum et al., 2020). Remarkably, P5C3 binding and neutralizing activity are not affected by these amino acid substitutions, due to its epitope position (Figure 5E). Additionally, the Q493K Spike mu-

tations did not impact the neutralizing activity of P5C3 on Spike-pseudotyped lentiviral particles despite structural evidence of direct interactions made between the antibody and Q493. These results suggest that the multiple contacts made by P5C3 with 21 Spike aa including the large cluster of interactions extending from A475 to G496 mitigate losses in affinity that would result from some individual changes. As well, mutations conferring resistance to some of these other mAbs are distal to the RBD/ACE2 interaction site (Figures 5D and 5E), with minimal effect on ACE2 binding and by extension on P5C3 recognition. Taken together, these observations suggest that virus variants harboring mutations in the P5C3-encoded epitope would suffer from an important fitness cost.
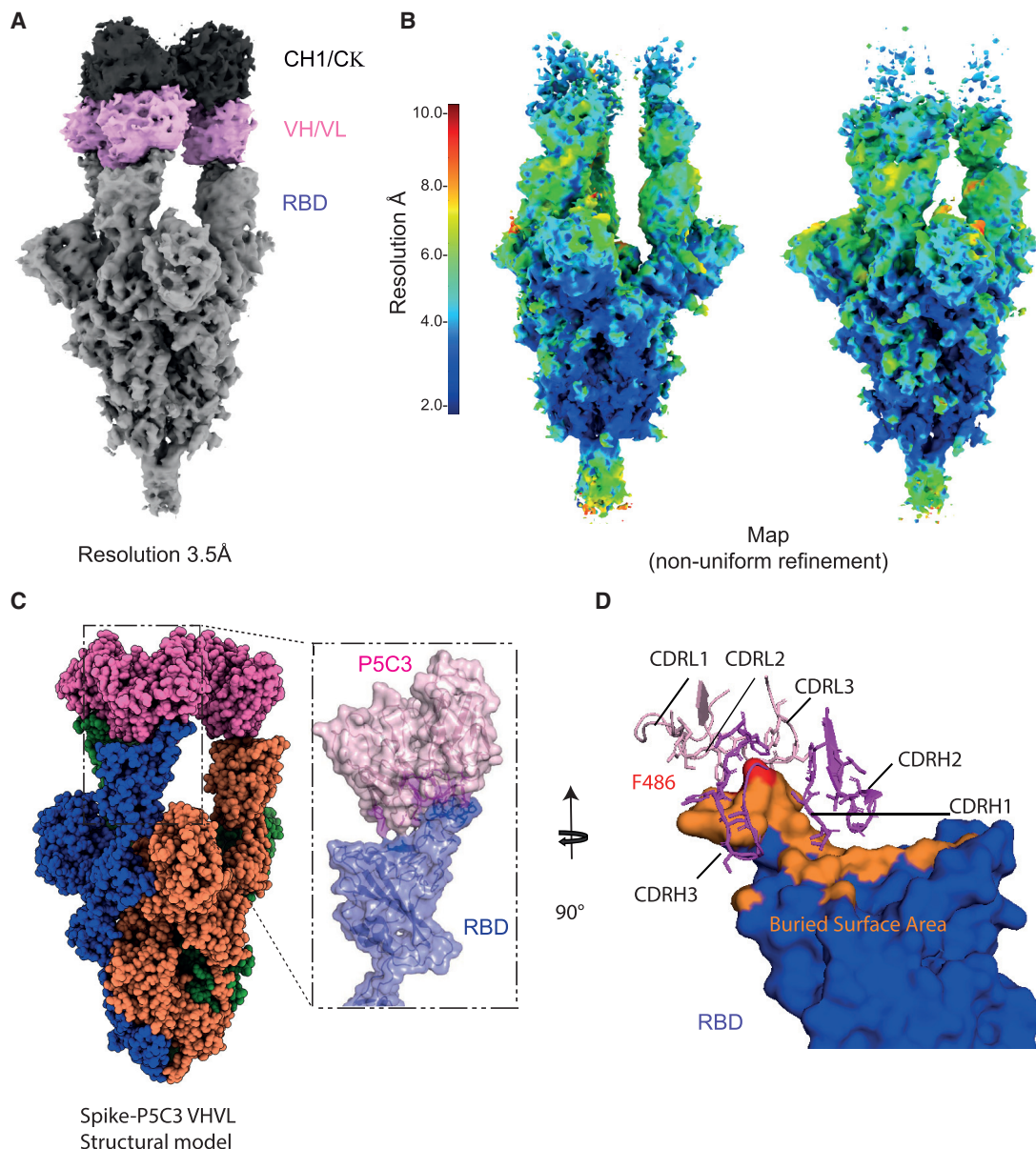
Figure 4. Structural characterization of P5C3 Fab bound to the SARS-CoV-2 spike

(A) Unsharpened cryo-EM map of P5C3 Fab in complex with SARS-CoV-2 spike at a resolution of 3.5 Å. The constant region of the Fab is colored in dark gray, the variable region of P5C3 in pink, and spike in gray.

(B) Resolution of the sharpened map is shown for the spike/Fab complex in two different poses. The spike core is below 3 Å, while the structure of P5C3 Fab in complex with the RBD is above 6 Å. Local resolution of P5C3 Fab and RBD after local refinement to reach 4.3 Å is shown. Mask and refinement are in Figure S4.

(C) SARS-CoV-2-P5C3 structure, with the spike protomers colored blue, green, and orange; the variable domain of the Fab is shown in pink.

(D) Buried surface area of the RBD bound by P5C3 Fabs shown in orange with the RBD F486 residue in red and the P5C3 CDR loops shown in pink and violet for the light and heavy chains, respectively.

P5C3 confers strong *in vivo* prophylactic protection from SARS-CoV-2 infection

Finally, we evaluated the neutralizing potency of P5C3 *in vivo* in a prophylactic hamster challenge model of SARS-CoV-2 infection. Animals were administered intraperitoneally 5.0, 1.0, or 0.5 mg/kg P5C3 or 5 mg/kg of an IgG1 isotype control and challenged 2 days later (day 0) with an intranasal inoculation of SARS-

CoV-2 virus (2.4×10^6 50% tissue culture infective dose [$TCID_{50}$]) (Figure 6A). Four days later, lungs from control animals contained between 10^4 and 5×10^6 $TCID_{50}$ per mg of tissue, whereas infectious virus was undetectable in lung from hamsters treated with 5.0 and 1.0 mg/kg P5C3, which displayed antibody plasma levels >12 μg/mL (ranging from 12.2 to 16.4 μg/mL in the 1.0 mg/kg dose) at the time of viral inoculation (Figures 6B and
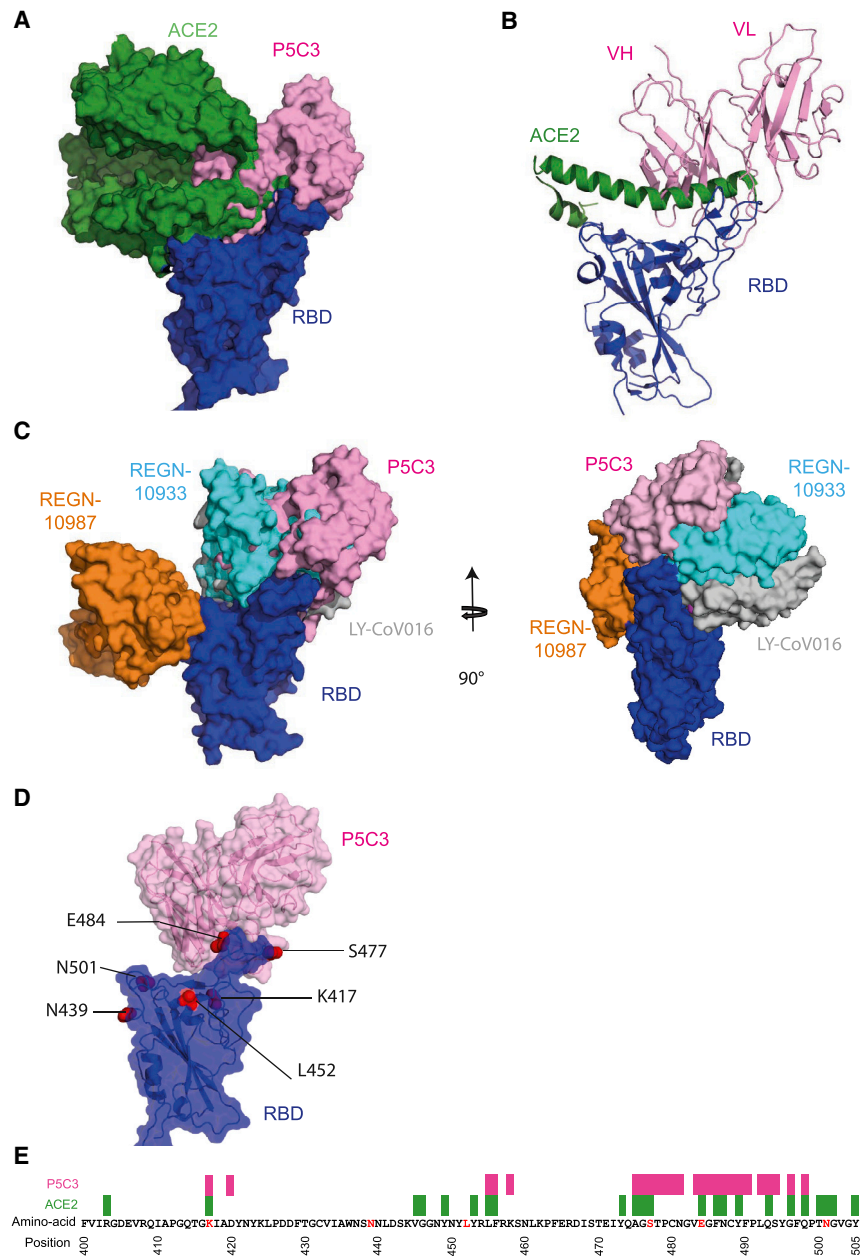
Figure 5. Structural characterization of P5C3 Fab bound to the SARS-CoV-2 spike

(A) Superimposed surface structure of ACE2 in green, P5C3 VHVL in pink on the RBD domain in blue.

(B) Cartoon representation of one RBD domain in blue, P5C3 VHVL in pink, and the helical domain of ACE2 contacted by the RBD in green.

(C) Superimposed surface structure of LY-CoV016 VHVL in gray, P5C3 VHVL in pink, REGN10987 VHVL in orange, and REGN10933 VHVL in cyan on the RBD domain in blue shown in front and side views.

(D) Common mutations of SARS-CoV-2 VOCs on RBD (K417, N439, L452, S477, E484, and N501) are shown as red spheres. P5C3 VHVL is shown in pink and RBD in blue with surfaces shown with transparency.

(E) Depiction of the epitope or interaction site present on the RBD. ACE2 interaction sites are shown in green and P5C3 in pink. Red letters indicate virus mutations present in virus variant circulating in the population.

through interaction with RBD in the open conformation. Distinct from other leader mAbs currently in the clinic of this class, including REGN10933 and LY-CoV555, P5C3 retains full activity against a panel of mutations found in circulating viral variants, including the B.1.351 containing the K417N/E484K/N501Y triple mutation in the RBD. Likewise, binding and neutralization assays performed with Spike mutations indicate that P5C3 will retain full potency against newly emerging variants, including P.1, CAL.20C, and B1.526. Structural characterization demonstrated that P5C3 binds the RBD with five CDR loops and occupying a large buried surface area that spans 600 Å^2. As such, the tight interaction of the antibody is spread over a large region and lacks particular binding hotspots that may be sensitive to mutations in the vicinity. These features could explain why individual or combinations of mutations including K417N and E484K at the edge of the P5C3 epitope do not influence its neutralizing activity. Moreover, the binding modes of P5C3 involving shared interactions with ACE2, contact site with the β5 and β6 antiparallel strands, and hydrophobic contacts with the RBD core suggest that mutations to escape P5C3 binding will invariably impact either affinity for ACE2 or folding properties of the RBD, both resulting in either reduced overall infectivity or an important fitness cost for the virus. As such, it is predicted that direct mutations in the RBD at the contact site with P5C3 will invariably impact the affinity for ACE2, resulting in a reduced overall infectivity and fitness of the virus.

Apart from the *in vitro* neutralization activity and binding properties, we also demonstrated that P5C3 exhibited an excellent
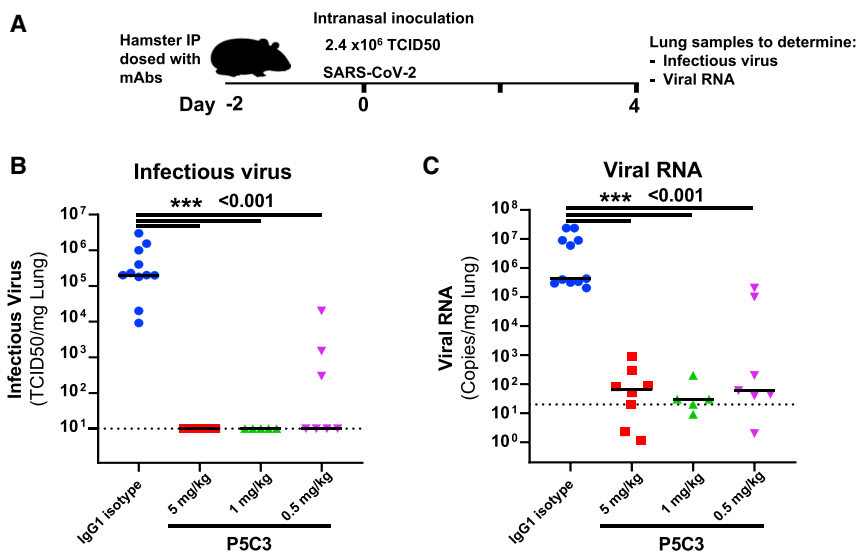
6C). Animals administered 0.5 mg/kg P5C3 had median plasma antibody levels of 6.7 μg/mL, and four out of seven also exhibited undetectable infectious virus in the lung, while the remaining three showed an ∼2 log reduction in TCID$_{50}$/mg lung tissue compared to the isotype mAb-treated controls. Significant reduction of viral RNA levels was also observed in all P5C3-treated groups (p < 0.001) with a ∼4 log reduction in viral genome copies per mg of lung tissue compared to control animals.

DISCUSSION

In sum, we report the discovery of P5C3, a highly potent SARS-CoV-2 class I neutralizing antibody that blocks ACE2 binding

A

Hamster IP
dosed with
mAbs

Intranasal inoculation
2.4 x10^6 TCID50
SARS-CoV-2

Lung samples to determine:
- Infectious virus
- Viral RNA

Day -2   0   4

B

Infectious virus

*** <0.001

Infectious Virus
(TCID50/mg Lung)

IgG1 isotype   5 mg/kg   1 mg/kg   0.5 mg/kg

P5C3

C

Viral RNA

*** <0.001

Viral RNA
(Copies/mg lung)

IgG1 isotype   5 mg/kg   1 mg/kg   0.5 mg/kg

P5C3

Figure 6. P5C3 shows potent *in vivo* efficacy in the hamster challenge model for SARS-CoV-2 infection

(A) Overview of study design for the SARS-CoV-2 hamster challenge model.

(B and C) Median levels of infectious virus (B) or viral RNA copies/mg lung tissue in each of the study arms (C) are shown on day 4 post-inoculation with SARS-CoV-2 virus. A total of five to eight hamsters were used per P5C3 treatment arm. Non-parametric Mann-Whitney U tests were used to evaluate the statistical difference between the treatment conditions. ***p < 0.001.

for RBD binding and forms direct contacts between CDR H1 G53-S54 and RBD β6 chain Q493, while these interactions are lacking for S2E12.

The proportion of the population receiving COVID-19 vaccines is continually increasing in many countries with a corresponding reduced rate of infections and hospitalizations. However, preliminary reports indicate that pre-existing natural immunity against the wild-type n-Cov19 is poorly effective against the VOCs as indicated by the large proportion of re-infection in geographic areas where there is wide circulation of the VOCs. Furthermore, the efficacy of several vaccines seems to be substantially affected by VOCs such as AZD1222, BNT162b2, and mRNA-1273 (Collier et al., 2021; Garcia-Beltran et al., 2021), and the durability of the persistence of protective immune responses induced by vaccination remains to be determined. More importantly, a significant portion of the population, quantified in several millions, with primary or acquired immunodeficiency as well as those receiving immunosuppressive treatments such as organ transplant recipients, cancer patients, and patients with systemic inflammatory diseases, notably undergoing B cell depletion therapy, do not mount a protective humoral immune response following vaccination. For these vulnerable individuals, passive immunization two to three times per year with the extended half-life P5C3 LS represents a very attractive treatment option (Chen et al., 2021a; Mohammed et al., 2020; Weinreich et al., 2021). With its potent neutralizing properties against all Spike mutations and SARS-CoV-2 variants identified so far and the demonstrated *in vivo* prophylactic protection in the hamster challenge model, P5C3 represents a best-in-class anti-SARS-CoV-2 antibody for use in the prophylactic setting.

in vivo prophylactic protection in the hamster challenge model. A 1 mg/kg dose, which correlated with P5C3 plasma concentrations of 12.2–16.4 μg/mL, completely suppressed the detection of infectious virus in the lung. Furthermore, a strong ~4 log reduction in viral RNA was observed in 5.0, 1.0, and 0.5 mg/kg P5C3 treatment arms.

Despite the excellent neutralization profile of P5C3 against current circulating variants, development of resistance is always a possibility when a specific selection pressure is applied to a virus. With SARS-CoV-2, the millions of infected individuals worldwide, the detection of viral quasi-species in infected individuals, the enhancement of viral mutations observed in immunocompromised subjects, and the worrisome occurrence of inter-species virus transmission all provide opportunities for the virus to evolve escape mutations. Interestingly, P5C3 does not compete for RBD binding with several other classes of neutralizing antibodies including REGN10987 and S309. As such, either of these antibodies or others of similar binding classes could be used in combination with P5C3 to exert both a more potent neutralizing activity and a higher barrier for the development of resistance.

Interestingly, antibodies sharing similar variable genetic region rearrangements (also called public antibodies) were isolated from several SARS-CoV-2-infected individuals (Robbiani et al., 2020; Tortorici et al., 2020). A few previously characterized SARS-CoV-2 neutralizing antibodies display features reminiscent of P5C3, including the presence of an intra-loop disulfide bond between adjacent Cys residues within CDR H3 (Kreer et al., 2020; Tortorici et al., 2020; Wang et al., 2021a). To date, several mAbs using the VH1-58 allele were reported (Mohammed et al., 2020), suggesting that P5C3 might belong to a public antibody family (shared among infected donors). The only mAb with the same VH structurally characterized is S2E12 (PDB 7K4N) (Chen et al., 2021b; Tortorici et al., 2020). However, P5C3 uses a different JH segment (IGHJ2*01), its light chain is distinct, and structural superimposition of the two Fabs demonstrate discrete binding conformations where P5C3 uses CDR H2

STAR★METHODS

Detailed methods are provided in the online version of this paper and include the following:

- KEY RESOURCES TABLE
- RESOURCE AVAILABILITY
  - Lead contact
  - Materials availability
  - Data and code availability

AUTHOR CONTRIBUTIONS

C.F. designed the strategy for isolating and profiling anti-Spike antibodies, coordinated all of the research activities, analyzed the data, wrote the initial draft of the manuscript, and contributed to the editing of the manuscript. P.T. established and performed the live SARS-CoV-2 virus cytopathic effect neutralization assay, designed the Spike protein mutations and cloning, analyzed the results, and contributed to the editing of the manuscript. L.P. coordinated the cryo-EM analysis, analyzed the structural data, wrote the manuscript structural section, and contributed to the editing of the manuscript. L.E.-L. performed the B cell sorting, immortalization, and binding studies; A.F. and E.L. performed VH and HL mAb cloning; J.C. performed binding studies and pseudoviral assays; C.P. performed mAb quantitation from *in vivo* studies and other binding studies; V.S.J. performed Fab preparation; F.F. performed mAb purification, mAb characterization, and molecular biology; M.D. performed the hFcRn PK studies; A.N. helped with antigen-specific B cell staining; M.F. performed antibody sequence analysis; B.-J.B. and W.D. provided proteins, PV vectors, and external testing of mAbs; C.R. performed site-directed mutagenesis of the Spike constructs; Y.L. and R.L. provided *in vivo* study designs; F.P., K.L., and the Protein Production and Structure Core Facility at the EPFL produced and purified the trimer S proteins; D.D. set up cryo-EM conditions for automated acquisition; R.A., P.L., C.S.F., L.V., G.V., and J.N. performed hamster studies; and G.P. and D.T. conceived the study design, analyzed the results, and wrote the manuscript.

DECLARATION OF INTERESTS

C.F., P.T., G.P., and D.T declare that they are co-inventors on a patent application titled "Neutralizing antibodies and use thereof in the treatment of SARS-CoV-2 infection" with filing number PCT/IB2021/050621 that covers newly identified antibodies described in this manuscript. The remaining authors declare no competing interests.

INCLUSION AND DIVERSITY

We worked to ensure diversity in experimental samples through the selection of the cell lines. One or more of the authors of this paper self-identifies as an underrepresented ethnic minority in science. The author list of this paper includes contributors from the location where the research was conducted who participated in the data collection, design, analysis, and/or interpretation of the work.

REFERENCES

Abrams, E.M., and Szefler, S.J. (2020). COVID-19 and the impact of social determinants of health. Lancet Respir. Med. *8*, 659–661.

Adams, P.D., Afonine, P.V., Bunkóczi, G., Chen, V.B., Davis, I.W., Echols, N., Headd, J.J., Hung, L.W., Kapral, G.J., Grosse-Kunstleve, R.W., et al. (2010). PHENIX: A comprehensive Python-based system for macromolecular structure solution. Acta Crystallogr. D Biol. Crystallogr. *66*, 213–221.

Barad, B.A., Echols, N., Wang, R.Y., Cheng, Y., DiMaio, F., Adams, P.D., and Fraser, J.S. (2015). EMRinger: Side chain-directed model and map validation for 3D cryo-electron microscopy. Nat. Methods *12*, 943–946.

Barnes, C.O., West, A.P., Jr., Huey-Tubman, K.E., Hoffmann, M.A.G., Sharaf, N.G., Hoffman, P.R., Koranda, N., Gristick, H.B., Gaebler, C., Muecksch, F., et al. (2020). Structures of human antibodies bound to SARS-CoV-2 spike reveal common epitopes and recurrent features of antibodies. Cell *182*, 828–842.e16.

Baum, A., Fulton, B.O., Wloga, E., Copin, R., Pascal, K.E., Russo, V., Giordano, S., Lanza, K., Negron, N., Ni, M., et al. (2020). Antibody cocktail to SARS-CoV-2 spike protein prevents rapid mutational escape seen with individual antibodies. Science *369*, 1014–1018.

Boudewijns, R., Thibaut, H.J., Kaptein, S.J.F., Li, R., Vergote, V., Seldeslachts, L., Van Weyenbergh, J., De Keyzer, C., Bervoets, L., Sharma, S., et al. (2020). STAT2 signaling restricts viral dissemination but drives severe pneumonia in SARS-CoV-2 infected hamsters. Nat. Commun. *11*, 5838.

Chen, V.B., Arendall, W.B., 3rd, Headd, J.J., Keedy, D.A., Immormino, R.M., Kapral, G.J., Murray, L.W., Richardson, J.S., and Richardson, D.C. (2010).

MolProbity: All-atom structure validation for macromolecular crystallography. Acta Crystallogr. D Biol. Crystallogr. *66*, 12–21.

Chen, P., Nirula, A., Heller, B., Gottlieb, R.L., Boscia, J., Morris, J., Huhn, G., Cardona, J., Mocherla, B., Stosor, V., et al.; BLAZE-1 Investigators (2021a). SARS-CoV-2 neutralizing antibody LY-CoV555 in outpatients with Covid-19. N. Engl. J. Med. *384*, 229–237.

Chen, R.E., Zhang, X., Case, J.B., Winkler, E.S., Liu, Y., VanBlargan, L.A., Liu, J., Errico, J.M., Xie, X., Suryadevara, N., et al. (2021b). Resistance of SARS-CoV-2 variants to neutralization by monoclonal and serum-derived polyclonal antibodies. Nat. Med. *27*, 717–726.

Collier, D.A., De Marco, A., Ferreira, I.A.T.M., Meng, B., Datir, R.P., Walls, A.C., Kemp, S.A., Bassi, J., Pinto, D., Silacci-Fregni, C., et al.; CITIID-NIHR Bio-Resource COVID-19 Collaboration; COVID-19 Genomics UK (COG-UK) Consortium (2021). Sensitivity of SARS-CoV-2 B.1.1.7 to mRNA vaccine-elicited antibodies. Nature *593*, 136–141.

Crawford, K.H.D., Eguia, R., Dingens, A.S., Loes, A.N., Malone, K.D., Wolf, C.R., Chu, H.Y., Tortorici, M.A., Veesler, D., Murphy, M., et al. (2020). Protocol and reagents for pseudotyping lentiviral particles with SARS-CoV-2 spike protein for neutralization assays. Viruses *12*, E513.

Davies, N.G., Abbott, S., Barnard, R.C., Jarvis, C.I., Kucharski, A.J., Munday, J.D., Pearson, C.A.B., Russell, T.W., Tully, D.C., Washburne, A.D., et al.; CMMID COVID-19 Working Group; COVID-19 Genomics UK (COG-UK) Consortium (2021). Estimated transmissibility and impact of SARS-CoV-2 lineage B.1.1.7 in England. Science *372*, eabg3055.

Emsley, P., Lohkamp, B., Scott, W.G., and Cowtan, K. (2010). Features and development of Coot. Acta Crystallogr. D Biol. Crystallogr. *66*, 486–501.

Fenwick, C., Croxatto, A., Coste, A.T., Pojer, F., André, C., Pellaton, C., Farina, A., Campos, J., Hacker, D., Lau, K., et al. (2021a). Changes in SARS-CoV-2 Spike versus nucleoprotein antibody responses impact the estimates of infections in population-based seroprevalence studies. J. Virol. *95*, e01828-20.

Fenwick, C., Turelli, P., Pellaton, C., Farina, A., Campos, J., Raclot, C., Pojer, F., Cagno, V., Pantaleo, G., and Trono, D. (2021b). A multiplexed high-throughput neutralization assay reveals a lack of activity against multiple variants after SARS-CoV-2 infection. medRxiv. https://doi.org/10.1101/2021.04.08.21255150.

Garcia-Beltran, W.F., Lam, E.C., St Denis, K., Nitido, A.D., Garcia, Z.H., Hauser, B.M., Feldman, J., Pavlovic, M.N., Gregory, D.J., Poznansky, M.C., et al. (2021). Multiple SARS-CoV-2 variants escape neutralization by vaccine-induced humoral immunity. Cell *184*, 2372–2383.e9.

Gautam, R., Nishimura, Y., Pegu, A., Nason, M.C., Klein, F., Gazumyan, A., Golijanin, J., Buckler-White, A., Sadjadpour, R., Wang, K., et al. (2016). A single injection of anti-HIV-1 antibodies protects against repeated SHIV challenges. Nature *533*, 105–109.

Goddard, T.D., Huang, C.C., Meng, E.C., Pettersen, E.F., Couch, G.S., Morris, J.H., and Ferrin, T.E. (2018). UCSF ChimeraX: Meeting modern challenges in visualization and analysis. Protein Sci. *27*, 14–25.

Hansen, J., Baum, A., Pascal, K.E., Russo, V., Giordano, S., Wloga, E., Fulton, B.O., Yan, Y., Koon, K., Patel, K., et al. (2020a). Studies in humanized mice and convalescent humans yield a SARS-CoV-2 antibody cocktail. Science *369*, 1010–1014.

Hansen, J., Baum, A., Pascal, K.E., Russo, V., Giordano, S., Wloga, E., Fulton, B.O., Yan, Y., Koon, K., Patel, K., et al. (2020b). Studies in humanized mice and convalescent humans yield a SARS-CoV-2 antibody cocktail. Science *369*, 1010–1014.

Hoffmann, M., Zhang, L., Krüger, N., Graichen, L., Kleine-Weber, H., Hofmann-Winkler, H., Kempf, A., Nessler, S., Riggert, J., Winkler, M.S., et al. (2021). SARS-CoV-2 mutations acquired in mink reduce antibody-mediated neutralization. Cell Rep. *35*, 109017.

Jones, B.E., Brown-Augsburger, P.L., Corbett, K.S., Westendorf, K., Davies, J., Cujec, T.P., Wiethoff, C.M., Blackbourne, J.L., Heinz, B.A., Foster, D., et al. (2020). LY-CoV555, a rapidly isolated potent neutralizing antibody, provides protection in a non-human primate model of SARS-CoV-2 infection. bioRxiv. https://doi.org/10.1101/2020.09.30.318972.

Kaptein, S.J.F., Jacobs, S., Langendries, L., Seldeslachts, L., Ter Horst, S., Liesenborghs, L., Hens, B., Vergote, V., Heylen, E., Barthelemy, K., et al. (2020). Favipiravir at high doses has potent antiviral activity in SARS-CoV-2-infected hamsters, whereas hydroxychloroquine lacks activity. Proc. Natl. Acad. Sci. USA *117*, 26955–26965.

Korber, B., Fischer, W.M., Gnanakaran, S., Yoon, H., Theiler, J., Abfalterer, W., Hengartner, N., Giorgi, E.E., Bhattacharya, T., Foley, B., et al.; Sheffield COVID-19 Genomics Group (2020). Tracking changes in SARS-CoV-2 Spike: evidence that D614G increases infectivity of the COVID-19 virus. Cell *182*, 812–827.e19.

Kreer, C., Zehner, M., Weber, T., Ercanoglu, M.S., Gieselmann, L., Rohde, C., Halwe, S., Korenkov, M., Schommers, P., Vanshylla, K., et al. (2020). Longitudinal Isolation of Potent near-germline SARS-CoV-2-neutralizing antibodies from COVID-19 patients. Cell *182*, 843–854.e12.

Lan, J., Ge, J., Yu, J., Shan, S., Zhou, H., Fan, S., Zhang, Q., Shi, X., Wang, Q., Zhang, L., and Wang, X. (2020). Structure of the SARS-CoV-2 spike receptor-binding domain bound to the ACE2 receptor. Nature *581*, 215–220.

Mastronarde, D.N. (2005). Automated electron microscope tomography using robust prediction of specimen movements. J. Struct. Biol. *152*, 36–51.

Meyer, L., López, T., Espinosa, R., Arias, C.F., Vollmers, C., and DuBois, R.M. (2019). A simplified workflow for monoclonal antibody sequencing. PLoS ONE *14*, e0218717.

Mohammed, A.H., Blebil, A., Dujaili, J., and Rasool-Hassan, B.A. (2020). The risk and impact of COVID-19 pandemic on immunosuppressed patients: Cancer, HIV, and solid organ transplant recipients. AIDS Rev. *22*, 151–157.

Ozono, S., Zhang, Y., Ode, H., Sano, K., Tan, T.S., Imai, K., Miyoshi, K., Kishigami, S., Ueno, T., Iwatani, Y., et al. (2021). SARS-CoV-2 D614G spike mutation increases entry efficiency with enhanced ACE2-binding affinity. Nat. Commun. *12*, 848.

Pettersen, E.F., Goddard, T.D., Huang, C.C., Couch, G.S., Greenblatt, D.M., Meng, E.C., and Ferrin, T.E. (2004). UCSF Chimera—A visualization system for exploratory research and analysis. J. Comput. Chem. *25*, 1605–1612.

Piccoli, L., Park, Y.J., Tortorici, M.A., Czudnochowski, N., Walls, A.C., Beltramello, M., Silacci-Fregni, C., Pinto, D., Rosen, L.E., Bowen, J.E., et al. (2020). Mapping neutralizing and immunodominant sites on the SARS-CoV-2 spike receptor-binding domain by structure-guided high-resolution serology. Cell *183*, 1024–1042.e21.

Pinto, D., Park, Y.J., Beltramello, M., Walls, A.C., Tortorici, M.A., Bianchi, S., Jaconi, S., Culap, K., Zatta, F., De Marco, A., et al. (2020). Cross-neutralization of SARS-CoV-2 by a human monoclonal SARS-CoV antibody. Nature *583*, 290–295.

Punjani, A., Rubinstein, J.L., Fleet, D.J., and Brubaker, M.A. (2017). cryo-SPARC: Algorithms for rapid unsupervised cryo-EM structure determination. Nat. Methods *14*, 290–296.

Rappazzo, C.G., Tse, L.V., Kaku, C.I., Wrapp, D., Sakharkar, M., Huang, D., Deveau, L.M., Yockachonis, T.J., Herbert, A.S., Battles, M.B., et al. (2020). An engineered antibody with broad protective efficacy in murine models of SARS and COVID-19. bioRxiv. https://doi.org/10.1101/2020.11.17.385500.

Robbiani, D.F., Gaebler, C., Muecksch, F., Lorenzi, J.C.C., Wang, Z., Cho, A., Agudelo, M., Barnes, C.O., Gazumyan, A., Finkin, S., et al. (2020). Convergent antibody responses to SARS-CoV-2 in convalescent individuals. Nature *584*, 437–442.

Rosenthal, P.B., and Henderson, R. (2003). Optimal determination of particle orientation, absolute hand, and contrast loss in single-particle electron cryomicroscopy. J. Mol. Biol. *333*, 721–745.

Sanchez-Felipe, L., Vercruysse, T., Sharma, S., Ma, J., Lemmens, V., Van Looveren, D., Arkalagud Javarappa, M.P., Boudewijns, R., Malengier-Devlies, B., Liesenborghs, L., et al. (2021). A single-dose live-attenuated YF17D-vectored SARS-CoV-2 vaccine candidate. Nature *590*, 320–325.

Shi, R., Shan, C., Duan, X., Chen, Z., Liu, P., Song, J., Song, T., Bi, X., Han, C., Wu, L., et al. (2020). A human neutralizing antibody targets the receptor-binding site of SARS-CoV-2. Nature *584*, 120–124.

Smith, K., Garman, L., Wrammert, J., Zheng, N.Y., Capra, J.D., Ahmed, R., and Wilson, P.C. (2009). Rapid generation of fully human monoclonal antibodies specific to a vaccinating antigen. Nat. Protoc. *4*, 372–384.

Starr, T.N., Greaney, A.J., Addetia, A., Hannon, W.W., Choudhary, M.C., Dingens, A.S., Li, J.Z., and Bloom, J.D. (2021). Prospective mapping of viral mutations that escape antibodies used to treat COVID-19. Science *371*, 850–854.

Sudre, C.H., Murray, B., Varsavsky, T., Graham, M.S., Penfold, R.S., Bowyer, R.C., Pujol, J.C., Klaser, K., Antonelli, M., Canas, L.S., et al. (2021). Attributes and predictors of long COVID. Nat. Med. *27*, 626–631.

Thi Nhu Thao, T., Labroussaa, F., Ebert, N., V'kovski, P., Stalder, H., Portmann, J., Kelly, J., Steiner, S., Holwerda, M., Kratzel, A., et al. (2020). Rapid reconstruction of SARS-CoV-2 using a synthetic genomics platform. Nature *582*, 561–565.

Thomson, E.C., Rosen, L.E., Shepherd, J.G., Spreafico, R., da Silva Filipe, A., Wojcechowskyj, J.A., Davis, C., Piccoli, L., Pascall, D.J., Dillen, J., et al.; ISARIC4C Investigators; COVID-19 Genomics UK (COG-UK) Consortium (2021). Circulating SARS-CoV-2 spike N439K variants maintain fitness while evading antibody-mediated immunity. Cell *184*, 1171–1187.e20.

Tortorici, M.A., Beltramello, M., Lempp, F.A., Pinto, D., Dang, H.V., Rosen, L.E., McCallum, M., Bowen, J., Minola, A., Jaconi, S., et al. (2020). Ultrapotent human antibodies protect against SARS-CoV-2 challenge via multiple mechanisms. Science *370*, 950–957.

Traggiai, E., Becker, S., Subbarao, K., Kolesnikova, L., Uematsu, Y., Gismondo, M.R., Murphy, B.R., Rappuoli, R., and Lanzavecchia, A. (2004). An efficient method to make human monoclonal antibodies from memory B cells: Potent neutralization of SARS coronavirus. Nat. Med. *10*, 871–875.

Volz, E., Mishra, S., Chand, M., Barrett, J.C., Johnson, R., Geidelberg, L., Hinsley, W.R., Laydon, D.J., Dabrera, G., O'Toole, Á., et al.; COVID-19 Genomics UK (COG-UK) consortium (2021). Assessing transmissibility of SARS-CoV-2 lineage B.1.1.7 in England. Nature *593*, 266–269.

Walls, A.C., Park, Y.-J., Tortorici, M.A., Wall, A., McGuire, A.T., and Veesler, D. (2020). Structure, function, and antigenicity of the SARS-CoV-2 spike glycoprotein. Cell *181*, 281–292.e6.

Wang, C., Li, W., Drabek, D., Okba, N.M.A., van Haperen, R., Osterhaus, A.D.M.E., van Kuppeveld, F.J.M., Haagmans, B.L., Grosveld, F., and Bosch, B.J. (2020a). A human monoclonal antibody blocking SARS-CoV-2 infection. Nat. Commun. *11*, 2251.

Wang, Y., Liu, M., and Gao, J. (2020b). Enhanced receptor binding of SARS-CoV-2 through networks of hydrogen-bonding and hydrophobic interactions. Proc. Natl. Acad. Sci. USA *117*, 13967–13974.

Wang, L., Zhou, T., Zhang, Y., Yang, E.S., Schramm, C.A., Shi, W., Pegu, A., Oloninyi, O.K., Ransier, A., Darko, S., et al. (2021a). Antibodies with potent and broad neutralizing activity against antigenically diverse and highly transmissible SARS-CoV-2 variants. bioRxiv. https://doi.org/10.1101/2021.02.25.432969.

Wang, P., Nair, M.S., Liu, L., Iketani, S., Luo, Y., Guo, Y., Wang, M., Yu, J., Zhang, B., Kwong, P.D., et al. (2021b). Antibody resistance of SARS-CoV-2 variants B.1.351 and B.1.1.7. Nature *593*, 130–135.

Weinreich, D.M., Sivapalasingam, S., Norton, T., Ali, S., Gao, H., Bhore, R., Musser, B.J., Soo, Y., Rofail, D., Im, J., et al.; Trial Investigators (2021). REGN-COV2, a neutralizing antibody cocktail, in outpatients with Covid-19. N. Engl. J. Med. *384*, 238–251.

Wrapp, D., Wang, N., Corbett, K.S., Goldsmith, J.A., Hsieh, C.-L., Abiona, O., Graham, B.S., and McLellan, J.S. (2020a). Cryo-EM structure of the 2019-nCoV spike in the prefusion conformation. Science *367*, 1260–1263.

Wrapp, D., Wang, N., Corbett, K.S., Goldsmith, J.A., Hsieh, C.L., Abiona, O., Graham, B.S., and McLellan, J.S. (2020b). Cryo-EM structure of the 2019-nCoV spike in the prefusion conformation. Science *367*, 1260–1263.

Zalevsky, J., Chamberlain, A.K., Horton, H.M., Karki, S., Leung, I.W., Sproule, T.J., Lazar, G.A., Roopenian, D.C., and Desjarlais, J.R. (2010). Enhanced antibody half-life improves in vivo activity. Nat. Biotechnol. *28*, 157–159.

Zhou, P., Yang, X.L., Wang, X.G., Hu, B., Zhang, L., Zhang, W., Si, H.R., Zhu, Y., Li, B., Huang, C.L., et al. (2020). A pneumonia outbreak associated with a new coronavirus of probable bat origin. Nature *579*, 270–273.

Zhou, D., Dejnirattisai, W., Supasa, P., Liu, C., Mentzer, A.J., Ginn, H.M., Zhao, Y., Duyvesteyn, H.M.E., Tuekprakhon, A., Nutalai, R., et al. (2021). Evidence of escape of SARS-CoV-2 variant B.1.351 from natural and vaccine-induced sera. Cell *184*, 2348–2361.e6.

STAR★METHODS

KEY RESOURCES TABLE

REAGENT or RESOURCE AVAILABILITY	SOURCE	IDENTIFIER
Antibodies		
P5C3 human monoclonal antibody	This paper	N/A
Mouse anti-human CD19 APC-Cy7	BD Biosciences	Cat#557791, RRID: AB_396873
Mouse anti-human CD3-BV510	BD Biosciences	Cat#563109, RRID: AB_2732053
Mouse anti-human IgM-FITC	Biolegend	Cat#314506, RRID: AB_493009
Mouse anti-human IgD PE-CF594	BD Biosciences	Cat#562540, RRID: AB_11153129
Mouse anti-human CD27-APC	BD Biosciences	Cat#558664; RRID: AB_1645457
Mouse anti-human CD38-V450	BD Biosciences	Cat#646851, RRID: AB_1937282
REGN10987	Hansen et al., 2020b	N/A
REGN10933	Hansen et al., 2020b	N/A
S309	Pinto et al., 2020	N/A
Bacterial and virus strains		
SARS-CoV-2	Geneva University Hospitals	hCoV-19/Switzerland/ GE9586
SARS-Cov-2 Mink-related variant	Statens Serum Institute	hCoV-19/Denmark/ DCGC-9495/2020
SARS-Cov2 recombinant clone D614G	Institute of virology and immunology (Thi Nhu Thao et al., 2020)	N/A
SARS-Cov2 recombinant clone B1.1.7	Institute of virology and immunology	N/A
SARS-Cov2 recombinant clone B1.351 Spike	Institute of virology and immunology	N/A
NEB 5-alpha High Efficiency Competent *E. coli* bacteria	New England Biolabs	Cat# C2987H
Chemicals, peptides, and recombinant proteins		
Recombinant trimeric Spike of SARS-Cov-2	Fenwick et al., 2021b	N/A
Recombinant trimeric Spike variants	This paper and Fenwick et al. (2021b)	N/A
D-desthiobiotin	Sigma	Cat#71610
RPMI medium	GIBCO, Life Technologies	Cat#61870-010
GlutaMAX™ supplement	ThermoFisher	Cat#35050061
Penicillin-Streptomycin	GIBCO, Life Technologies	Cat#15070-063
Fetal Bovine Serum (FBS)	ThermoFisher	Cat#10500064
Minimum Essential Medium Eagle	Sigma Aldrich	Cat#M2279
MEM Non-Essential Amino Acids Solution	GIBCO, Life Technologies	Cat#11140050
PEI MAX	Polysciences	Cat#49553-93-7
ProCHO5 medium	Lonza	Cat#BELN12-766Q
Human IL-2	Miltenyi Biotec	Cat#130-097-742
Human IL-21	Miltenyi Biotec	Cat#130-095-768
Human IL6	Miltenyi Biotec	Cat#130-095-352
TLR9 agonist CpG 2006	Invivogen	Cat#tlrl-2006
2-bêta-mercaptoethanol	Sigma	Cat#M6250-10ML
Critical commercial assays		
HIV p24 antigen ELISA	Zeptometrix	Cat#0801111
ONE-step Luciferase assay	BPS Bioscience	Cat#60690
Deposited data		
Structural model: Full spike with P5C3 Fab	PDB	PDB ID: 7P40 EMD-13190
Structural model: Local refinement RBD+Fab	PDB	PDB ID: 7PHG EMD-13415

Continued

REAGENT or RESOURCE AVAILABILITY	SOURCE	IDENTIFIER
Experimental model and subject details		
Experimental models: Cell lines		
Human embryonic kidney cells (HEK293T)	ATCC	Cat#CRL-3216, RRID:CVCL_0063
ExpiCHO cells	ThermoFischer	Cat#A29127, RRID:CVCL_5J31
VeroE6	ATCC	Cat#CRL-1586, RRID:CVCL_0574
B95-8 cells	ATCC	Cat#CRL-1612, RRID:CVCL_1953
3T3ms CD40L cells	NIH AIDS	Cat#12535, RRID:CVCL_1H10
HEK293T_ACE2	This paper and Fenwick et al. (2021b)	N/A
Oligonucleotides		
For recombinant trimeric Spikes constructs	Fenwick et al., 2021b	N/A
L452R recombinant trimeric Spike	This paper, microsynth	N/A
Recombinant DNA		
pCDH-EF1-MCS	System Biosciences	Cat#CD502A-1
pMD2.G	D. Trono	Addgene, Cat#12259, RRID:Addgene_12259
psPAX2	D. Trono	Addgene, Cat#12260, RRID:Addgene_12260
pCAGGS-SARS2-S D614G	Wang et al., 2021a	N/A
pMDL p.RRE	D.Trono	Addgene, Cat#12251
pRSV.Rev	D. Trono	Addgene, Cat#12253
pUltra-Chili-Luc vectors	M. Moore	Addgene, Cat#48688, RRID:Addgene_48688
pHAGE2-CMV-Luc-ZSgreen, Hgpm2, REV1b and Tat1b	Crawford et al., 2020	N/A
HDM-IDTSpike-fixK	Crawford et al., 2020	BEI NR-52514
HDM-IDTSpike-fixK-mutants	Fenwick et al., 2021b	N/A
2019-nCoV plasmid	Wrapp et al., 2020b	N/A
2019-nCoV mutants plasmids	This paper and Fenwick et al. (2021b)	N/A
Experimental models: Animal models		
Female hFcRn Tg32 mice of 12 weeks age.	Jackson laboratory	Stock No.014565
Female wild-type Syrian Golden hamsters (Mesocricetus auratus) 6 to 8 weeks of age.	Janvier Laboratories	Syrian Golden hamsters
COVID-19 patient biological samples		
B cells specific for SARS-CoV-2 Spike	Patient specific	ImmunoCov study
Software and algorithms		
FlowJo v10	FlowJo, LLC	https://www.flowjo.com/solutions/flowjo
GraphPad Prism 8.3.0	GraphPad	https://www.graphpad.com/
BioTek Gen5 v.3.0.3	BioTek	https://www.biotek.com/products/get-info/gen5-get-info.html
cryoSPARC v.3.0. 1	Punjani et al., 2017	https://cryosparc.com/
COOT	Emsley et al., 2010	https://www2.mrc-lmb.cam.ac.uk/personal/pemsley/coot/
UCSF Chimera	Pettersen et al., 2004	http://www.cgl.ucsf.edu/chimera/index.html
PHENIX	Adams et al., 2010	https://phenix-online.org/documentation/index.html
EM RINGER	Barad et al., 2015	https://github.com/fraser-lab/EMRinger
UCSF ChimeraX	Goddard et al., 2018	https://www.rbvi.ucsf.edu/chimerax/

Continued

REAGENT or RESOURCE AVAILABILITY	SOURCE	IDENTIFIER
Pymol	Schrödinger	https://pymol.org/2/
ImageJ software	National Institutes of Health	https://imagej.nih.gov
Other		
Streptactin	IBA	Cat#15728207
StrepTrap HP	Cytiva	Cat#28907546
Streptavidin-PE	BD Biosciences	Cat# 554061; RRID: AB_10053328
Live/Dead Cell staining - Aqua	Invitrogen	Cat#L34965

RESOURCE AVAILABILITY

Lead contact
Further information and requests for resources and reagents should be directed to and will be fulfilled by the Lead Contact, Giuseppe Pantaleo (Giuseppe.Pantaleo@CHUV.CH). E-mail subject title should be "CELL REPORTS_SARS-CoV-2 mAb REQUEST" to facilitate identification and processing of requests.

Materials availability
Reagent generated in this study will be made available on request, but we may require a payment and/or a completed Materials Transfer Agreement, which allows the use of the antibodies for non-commercial purposes but not their disclosure to third parties.

Data and code availability

- Data describe are available upon request and have been deposited at https://github.com/Laurent-9475/Cell-report and are publicly available as of the date of publication. The cryo-electron maps reconstruction of the Spike complex by Electron microscopy was deposited to the EMDataBank with the identifier EMD-13190 and EMD-13415.
- This paper does not report original code.
- Any additional information required to reanalyze the data reported in this paper is available from the lead contact upon request.

EXPERIMENTAL MODEL AND SUBJECT DETAILS

Study COVID-19 donors
Serum and blood mononuclear cell samples were from donors participating in the ImmunoCov study performed by the Immunology and Allergy Service, Lausanne University Hospital. Hospitalized donors selected for B cell immortalization studies consisted of six men and two women with mean ages of 51.5 and 52.4 years old, respectively. Study design and use of subject samples were approved by the Institutional Review Board of the Lausanne University Hospital and the 'Commission d'éthique du Canton de Vaud' (CER-VD).

Animals
Female hFcRn Tg32 mice used in the pharmacokinetic studies were of 12 weeks age were obtained from Jackson laboratory (Stock No.014565) and hosted at the conventional animal facility of Lausanne University (Epalinges site). All experiments were approved by the local Animal Care and Use Committee.

Wild-type Syrian Golden hamsters (Mesocricetus auratus) were purchased from Janvier Laboratories and were housed in ventilated isolator cages (IsoCage N Biocontainment System, Tecniplast) with *ad libitum* access to food and water and cage enrichment (wood block). The animals were acclimated for 4 days prior to study start. Housing conditions and experimental procedures were approved by the ethics committee of animal experimentation of KU Leuven (license P065-2020).

Cells and virus strains
Human embryonic kidney cells, HEK293T (ATCC Cat#CRL-3216) Cells were grown in Dulbecco's modified Eagle's medium (DMEM) supplemented with 10% heat-inactivated fetal bovine serum (FBS, Institut de Biotechnologies Jacques Boy), MEM non-essential amino acids (NEAA), 2 mM L-glutamine, 100 IU/ml penicillin, and 100 μg/ml streptomycin (GIBCO, Life Technologies). Cells were cultured at 37°C, 5% CO2 at 95% air atmosphere.

ExpiCHO cells (ThermoFischer, Cat#A29127) were cultured in ProCHO5 medium (Lonza). VeroE6 (ATCC,Cat#CRL-1586) were cultured in DMEM medium supplemented with 2% FBS and NEAA, 2 mM L-glutamine, 100 IU/ml penicillin, and 100 μg/ml strepto-mycin (GIBCO, Life Technologies).

B95-8 cells (ATCC, Cat#CRL-1612) were cultured in Roswell Park Memorial Institute 1640 (RPMI) medium (GIBCO, Life Technol-ogies) supplemented with 10% FBS, 100 IU/ml penicillin, and 100 μg/ml streptomycin (GIBCO, Life Technologies).

3T3ms CD40L cells were obtained from the NIH AIDS Reagent Repository (Cat#12535) and grown in the same medium and con-ditions as used for HEK293T cells.

SARS-Cov2 D614G (hCoV-19/Switzerland/GE9586, a kind gift from I. Ackerle, Geneva University Hospitals) and SARS-Cov2 Mink-related variant 16 (hCoV-19/Denmark/DCGC-9495/2020, a kind gift from A. Fomsgaard, Statens Serum Institute) are strains isolated from infected patients. Clones with the D614G mutation only, the mutations found in B.1.1.7 strain or in the B1.351 Spike were created by reverse genetics as previously described in Thi Nhu Thao et al. (2020). Viral stocks prepared in DMEM 2% FCS on VeroE6 cells were aliquoted, frozen and titrated by plaque assays on VeroE6 cells. All the biosafety level 3 procedures were approved by the Swiss Federal Office of Public Health.

The SARS-CoV-2 strain used in the hamster study, BetaCov/Belgium/GHB-03021/2020 (EPI ISL 109407976|2020-02-03), was recovered from a nasopharyngeal swab taken from an RT-qPCR confirmed asymptomatic patient who returned from Wuhan, China in the beginning of February 2020. A close relation with the prototypic Wuhan-Hu-1 2019-nCoV (GenBank accession 11 number MN908947.3) strain was confirmed by phylogenetic analysis. Infectious virus was isolated by serial passaging on HuH7 and Vero E6 cells (Boudewijns et al., 2020); passage 6 virus was used for the study described here. The titer of the virus stock was determined by end-point dilution on Vero E6 cells by the Reed and Muench method. Live virus-related work was conducted in the high-contain-ment A3 and BSL3+ facilities of the KU Leuven Rega Institute (3CAPS) under licenses AMV 30112018 SBB 219 2018 0892 and AMV 23102017 SBB 219 20170589 according to institutional guidelines.

METHOD DETAILS

Recombinant proteins

The Spike trimer was designed to mimic the native trimeric conformation of the protein *in vivo* and the expression vector was kindly provided by Prof. Jason McLellan, University of Texas, Austin. It encoded the prefusion ectodomain of the original 2019-Cov Spike with a C-terminal T4 foldon fusion domain to stabilize the trimer complex along with C-terminal 8x His and 2xStrep tags for affinity purification. The trimeric Spike protein was transiently expressed in suspension-adapted ExpiCHO cells (Thermo Fisher) in ProCHO5 medium (Lonza) at 5 x10^6 cells/mL using PEI MAX (Polysciences) for DNA delivery. At 1 h post-transfection, dimethyl sulfoxide (DMSO; AppliChem) was added to 2% (v/v). Following a 7-day incubation with agitation at 31°C and 4.5% CO_2, the cell culture me-dium was harvested and clarified using a 0.22 μm filter. The conditioned medium was loaded onto Streptactin (IBA) and StrepTrap HP (Cytiva) columns in tandem, washed with PBS, and eluted with 10 mM desthiobiotin in PBS. The purity of Spike trimers was deter-mined to be > 99% pure by SDS-PAGE analysis. Generation of Spike expression vectors encoding the mutations D614G, D614G plus K417N, N439K, L452R, S477N, E484K, N501Y or combinations thereof were generated by InFusion- mediated site directed muta-genesis using primers as previously described in Fenwick et al. (Fenwick et al., 2021b) and L452R: 5′-CAACTACAACTACCGG TACCGGCTGTTTC-3′. The B.1.1.7, B.1.351 and P.1 variant clones were generated by gene synthesis (Twist Biosciences). Spike protein for all mutants were produced and purified in an identical manner to the original 2019-CoV Spike protein. Biotinylation of Spike or RBD proteins was performed using the EZ-Link NHS-PEG4-Biotin (Life Technologies) using a 3-fold molar excess of reagent and using the manufacturer's protocol. Biotinylated proteins were buffer exchanged with PBS using an Amicon Ultra-0.5 with a 3 kDa molecular weight cut-off. Spike and RBD tetramers were prepared fresh before use and formed by combining biotinylated proteins with PE-conjugated Streptavidin (BD Biosciences) at a molar ratio of 4:1.

Antibody heavy and light chain sequences were integrated into the AbVec2.0-IGHG1,AbVec1.1-IGKC and AbVec1.1-IGLC2-XhoI vectors (Addgene) by synthetic gene synthesis (Twist biosciences). Antibodies produced by transient transfection of ExpiCHO cells (ThermoFisher) were purified as previously described (Fenwick et al., 2021b).

Binding studies with SARS-CoV-2 Spike

Luminex beads used for the serological and purified antibody binding assays were prepared by covalent coupling of SARS-CoV-2 proteins with MagPlex beads using the manufacturer's protocol with a Bio-Plex Amine Coupling Kit (Bio-Rad, France). Each of the SARS-CoV-2 Spike proteins expressed with different mutations were coupled with different colored MagPlex beads so that tests could be performed with a single protein bead per well or in a multiplexed Luminex binding assay. Binding curves with serial dilutions of serum samples or antibodies was performed as previously described in Fenwick et al., 2021a (Fenwick et al., 2021a) with percent binding to Spike trimer calculated using the formula: % binding = ([MFI Test dilution – MFI buffer negative control] / [MFI Max binding – MFI buffer negative control]) × 100). Serum dilution response inhibition curves were generated with GraphPad Prism 8.3.0 using Non Linear four parameter curve fitting analysis of the log (agonist) versus response. Competitive binding studies were performed by pre-incubating 25 μg/ml of the indicated competitor antibody with RBD coupled Luminex beads for 30 minutes. Biotinylated P5C3, REGN10933, REGN10987 or S309 antibodies (prepared as described above) were added to each well at 1 μg/ml followed by a further 20-minute incubation. Biotinylated antibody bound to RBD in the presence of competitor was stained with

Streptavidin-PE at a 1:1000 dilution (BD Biosciences) and analyzed on a 200 Bioplex instruments. COVID-19 serum samples from 40 donors were monitored for levels of IgG antibody binding to the SARS-CoV-2 Spike trimer in the Luminex bead based assay. Eight donors with the highest levels of anti-Spike antibody were selected for antigen specific B cell cloning studies.

Anti-Spike and RBD B cell sorting, immortalization, and cloning

Blood from the eight selected COVID-19 hospitalized donors at the Lausanne University Hospital were collected in EDTA tubes and the isolation of blood mononuclear cell was performed using Leucosep centrifuge tubes (Greiner Bio-one) prefilled with density gradient medium (Ficoll-PaqueTM PLUS, GE Healthcare) according to the manufacturer's instructions. Freshly isolated cells were resuspended in RPMI medium (GIBCO, Life Technologies) supplemented with 10% heat-inactivated fetal bovine serum (FBS) (Institut de Biotechnologies Jacques Boy), 100 IU/ml penicillin, and 100 μg/ml streptomycin (GIBCO, Life Technologies). Cell were stained for 30 minutes on ice with the cocktail of fluorescent conjugated antibodies containing anti-CD19 APC-Cy7, anti-CD3-BV510, anti-IgM-FITC, anti-IgD PE-CF594, anti-CD27-APC, anti-CD38-V450 (BD Biosciences) along with the pre-complexed Spike and RBD tetramers (2 μg in 100μl) coupled to PE-streptavidin (BD Biosciences). Cells were then stained with Aqua Live/Dead cell stain (Invitrogen) and viable Spike/RBD specific memory B cells (CD19+/IgM-/IgD-/CD27+) and plasmablasts (CD19+/IgM-/IgD-/CD27+/CD38hi) were sorted using a FACSAria instrument. B cell immortalization was performed as previously described (Traggiai et al., 2004). Briefly, antigen specific B cells were incubated for 2 hours at 37°C in complete RPMI medium that included a 1:3 dilution of EBV containing supernatant from B95-8 cells (ATCC) and was supplemented with 2 ng/ml IL-2, 10 ng/ml IL-21 and 10 ng/ml IL-6 (Miltenyi Biotec), 2.5 μg/mL TLR9 agonist CpG 2006 (Invivogen) and MEM Non-essential amino acids solution (GIBCO /Thermofisher). Cells were then counted and plated at 3 cells per well in a 384-well plate with 1000 cells per well of irradiated 3T3ms CD40L cells (NIH AIDS reagent program). B cells producing anti-Spike antibodies were determined by a Luminex binding assay (1165 wells total) and supernatants from positive wells was further profiled at 1:5 and 1:40 dilutions in a Spike-pseudotyped lentiviral neutralization assays as described below. For supernatants possessing the highest binding and neutralization activity for a given concentration of human IgG antibody, RNA was isolated with the RNeasy Micro Kit (QIAGEN) and cDNA generated using the SMARTScribe Reverse Transcriptase kit (Takara Bio) using human IgG constant region oligos (Smith et al., 2009) and the Template-switch oligo (5′ aagcagtgg-tatcaacgcagagtacatgrgrgr 3′) according to the manufacturer's protocol. Heavy and light chain variable regions were amplified using the universal forward primer (5′ aagcagtggtatcaacgcagag 3′) and reverse primers followed by a second round amplification with nested primer as previously described (Meyer et al., 2019) except for the used of 0.2mM dNTP Mix (Thermo Fisher Scientific) and 0.5U of Platinum Taq DNA Polymerase High Fidelity (Invitrogen). PCR products were separated on an agarose gel and heavy and light chain amplicon bands were excised, purified using the NucleoSpin Gel and PCR Clean-up Kit (NAGEL GmbH), ligated into the pGEM-T Easy Vector Systems (Promega) using 3U of T4 DNA Ligase (Promega). Ligated samples were transformed into NEB 5-alpha High Efficiency Competent *E. coli* bacteria (New England Biolabs) with inserts amplified the following day by colony PCR. Antibody Sanger sequencing was performed by Fasteris (Geneva, Switzerland) with the variable heavy and light chain sequences annotated with IgBLAST. Sequences for 103 paired heavy and light chains were integrated into the AbVec2.0-IGHG1,AbVec1.1-IGKC and AbVec1.1-IGLC2-XhoI vectors (Addgene) by synthetic gene synthesis (Twist biosciences). Antibodies produced by transient transfection of ExpiCHO cells (ThermoFisher) were purified as previously described (Fenwick et al., 2021b)().

SARS-CoV-2 live virus cell-based cytopathic effect neutralization assay

The day before infection VeroE6 cells were seeded in 96-well plates at a density of $1.25x10^4$ cells per well. Heat inactivated sera from patients were diluted 1:10 in DMEM 2% FCS in a separate 96-well plate. Four-fold dilutions were then prepared in DMEM 2% FCS in a final volume of 60 μl. Equal amounts of the different viruses (1500 plaque forming units)diluted in DMEM 2% FCS were added to the diluted sera at a 1:1 volume/volume ratio. The virus-serum mixture was incubated at 37°C for 1 hour then 100 μl of the mixture was subsequently added to the VeroE6 cells in duplicates. After 48 hours of incubation at 37°C cells were washed once with PBS and fixed with 4% formaldehyde solution for 30 minutes at room temperature. Cells were washed once with PBS and plates were put at 70°C for 15 minutes for a second inactivation. Staining was performed outside the BSL3 laboratory with 50 μl of 0.1% crystal violet solution for 20 minutes at RT. Wells were washed 3 times with water and plates were dried, scanned and analyzed for the density of live violet stained cells using ImageJ software (National Institutes of Health). For each 96-well plate, at least 4 wells were treated with a negative pool of sera from pre-pandemic healthy donors and 4 wells with virus only and used as negative and positive controls respectively. The percent inhibition of cytopathic effect of the virus was calculated using the formula: % Inhibition = ([cell density Test dilution – cell density with virus only] / [cell density negative control no virus infection – cell density with virus only]) × 100. Serum dilution response inhibition curves were generated with GraphPad Prism 8.3.0 using NonLinear four parameter curve fitting analysis of thelog(agonist) versusresponse. Neutralization EC_{50} and EC_{80} values were calculated using the GraphPad prism NonLinear four parameter curve fitting analysis.

Spike-pseudotyped lentivector production and neutralization assays

HDM-IDTSpike-fixK plasmid (BEI catalog number NR-52514, obtained from J.D. Bloom, Fred Hutchinson Cancer Research Center) encoding the Wuhan-Hu-1 (or 2019-nCoV) SARS-Cov2 Spike (GenBank NC_045512) was modified using QuickChange mutagenesis to generate mutants with D614G alone or in combination with A222V, N439K, S477N and E484K/N501Y and K417N/E484K/N501Y as previously described (Fenwick et al., 2021b). Spike-pseudotyped lentivectors were generated by

co-transfecting HDM-IDTSpike-fixK, pHAGE2-CMV-Luc-ZSgreen, Hgpm2, REV1b and Tat1b (a kind gift from J.D. Bloom, Fred Hutchinson Cancer Research Center) plasmids into 293T cells for 24 hours with the following ratio 3/9/2/2/2 (18 μg/ 56.7cm2 plate) using Fugene transfection reagent (Promega). The following day, cells were transferred in EpiSerf medium, and cell supernatants were collected after 8 hours and 16 hours. Harvested supernatants were pooled, clarified by low-speed centrifugation, filtered to remove cell debris and aliquoted. Pseudoviruses encoding Spike Q493K and S494P mutations were generated using the appropriate pCAGGS-SARS2-S D614G-d18 Spike mutant vectors (Wang et al., 2020a) co-transfected with pMDL p.RRE, pRSV.Rev and pUltra-Chili-Luc vectors (Addgene) into 293T cells in DMEM medium + 10% FCS using Fugene 6 (Promega) according to the manufacturer's protocol. Following a two day incubation in cell culture, pseudoviruses were harvested from the cell culture supernatant and treated as described above. In the pseudoviral neutralization assay, 293T cells stably expressing the ACE2 receptor were suspended in DMEM medium with 10% FCS and seeded at $1.0x10^4$ cells per well into 96-well plates. After 5 hours in cell culture at 37°C, three-fold dilutions of serum samples were prepared and pre-incubated with the same amount of each pseudovirus in a final volume of 100 μL in DMEM + 10% FCS. Following a further 1 hour incubation at 37°C, the pseudoviruses/serum mixture was added to the 293T ACE2 cells. After 48 hours of incubation at 37°C, a luciferase assay was performed to monitor pseudoviral infection, using the ONE-Step Luciferase assay system as recommended by the manufacturer (BPS Bioscience). Viral neutralization resulted in the reduction of the relative light units detected. Neutralization EC_{50} and EC_{80} values were calculated using the GraphPad prism NonLinear four parameter curve fitting analysis.

Cryo-EM sample preparation
For cryo-EM, P5C3 Fab with Spike D614G complexes (3 μL aliquot of Spike with Fab (1:4 molar ratio)) were almost immediately applied to a freshly glow-discharged Quantifoil holey carbon grids (R2.0/2.0, 200 mesh, copper) at 1 mg/ml and. The grids were placed in an automatic plunge freezing apparatus Vitrobot Mark IV (Thermo Fisher, Hillsboro, USA) to control humidity (100%) and temperature (22°C). The blotting time was set for 2.0-3.0 s using filter paper (grade 595, Ted Pella Inc.) before vitrification in liquid ethane.

Cryo-EM data collection and image processing
Dose-fractionated images (i.e., movies) were recorded with a FEI Titan Krios (Thermo Fisher), operated at 300kV, and equipped with a Gatan Quantum-LS energy filter (20 eV zero-loss energy filtration) followed by a Gatan K2 Summit direct electron detector. Images were recorded in counting mode, at a magnification yielding a physical pixel size of 0.82Å at the sample level. Images were automatically recorded with the SerialEM program (Mastronarde, 2005). A defocus range of 0.8-2.5 μm was applied with a nominal magnification of x105 000, corresponding to a calibrated pixel size of 0.82 Å/pixel and with a total dose of 38e/$Å^2$. All data processing was performed in cryoSPARC v.3.0.1, movie frame alignment, estimation of the microscope contrast-transfer function parameters, particle picking and extraction (extraction box size 600 pixels^2) were carried out using cryoSPARC v.3.0.1 (Punjani et al., 2017). Next, several round of reference-free 2D classification were performed to remove artifacts particles using cryoSPARC v.3.0.1 (Punjani et al., 2017). Approximately 2 million of particles were used to generate four *Ab initio* volumes were generated, with one class of 585 005 particles revealing an S-trimer complexed with 3 Fabs. The map of interest was processed by non-uniform refinement with C1 symmetry to generate a map with a resolution of 3.5Å. Next, to improve the Fab RBD interface resolution, a local refinement was performed with mask shown in Figure S4A. All procedures were carried out in cryoSPARC v3.1.0 (Punjani et al., 2017). The reported resolutions are based on the gold-standard Fourier shell correlation curves (FSC = 0.143) criterion (Rosenthal and Henderson, 2003).

Cryo-EM model building and analysis
UCSF Chimera (Pettersen et al., 2004) and Coot (Emsley et al., 2010) were used to fit atomic model (PDB ID: 7K4N) (Tortorici et al., 2020) into the cryo-EM map. The model was refined using iterative real-space refinements in PHENIX (Adams et al., 2010). After several round of real-space refinement, when visible side-chains orientations were manually adjusted in Coot (Emsley et al., 2010) to ensure energy-favored geometry. Analysis of Map and model was validated using MolProbity (Chen et al., 2010) and EMringer (Barad et al., 2015). Figures were generated using UCSF ChimeraX (Goddard et al., 2018) and PyMOL (Schrödinger, Inc).

Hamster challenge model SARS-CoV-2 infection
KU LEUVEN R&D has developed and validated a SARS-CoV-2 Syrian Golden hamster infection model that is suitable for the evaluation of potential antiviral activity of novel antibodies (Boudewijns et al., 2020; Kaptein et al., 2020; Sanchez-Felipe et al., 2021). The hamster infection model of SARS-CoV-2 has been described before (Boudewijns et al., 2020; Sanchez-Felipe et al., 2021). Female hamsters of 6-8 weeks old were administered IgG1 isotype control (5 mg/kg) or P5C3 (5 mg/kg, 1 mg/kg or 0.5 mg/kg) by intraperitoneal injection. Two days later, hamsters were anesthetized with ketamine/xylazine/atropine, blood samples were collected and animals were inoculated intranasally with 2.4×10^6 median tissue culture infectious dose ($TCID_{50}$) of SARS-CoV-2 (day 0). Hamsters were monitored for appearance, behavior and weight. Antibody concentrations present in the hamster plasma on day 0 of the study were performed using the Luminex assay described above with Spike trimer coupled beads and using purified P5C3 antibody to generate a standard curve. At day 4 post infection, hamsters were sacrificed and lung tissues were homogenized using bead disruption (Precellys) in 350 μL TRK lysis buffer (E.Z.N.A. Total RNA Kit, Omega Bio-tek) and centrifuged (10,000 rpm, 5 min) to pellet the cell

debris. RNA was extracted according to the manufacturer's instructions. Of 50 μL eluate, 4 μL was used as a template in RT-qPCR reactions. RT-qPCR was performed on a LightCycler96 platform (Roche) using the iTaq Universal Probes One-Step RT-qPCR kit (BioRad) with N2 primers and probes targeting the nucleocapsid (Boudewijns et al., 2020). Standards of SARS-CoV-2 cDNA (IDT) were used to express viral genome copies per mg tissue. For end-point virus titrations, lung tissues were homogenized using bead disruption (Precellys) in 350 μL minimal essential medium and centrifuged (10,000 rpm, 5min, $4^{\circ}C$) to pellet the cell debris. To quantify infectious SARS- CoV-2 particles, endpoint titrations were performed on confluent Vero E6 cells in 96- well plates. Viral titers were calculated by the Reed and Muench method using the Lindenbach calculator and were expressed as 50% tissue culture infectious dose ($TCID_{50}$) per mg tissue.

Pharmacokinetic studies in human FcRn transgenic mice

Pre-treatment sera was collected from each of the mice and the following day mice were administered 2 mg/kg of either P5C3 IgG1 or P5C3 IgG1 LS antibodies by retro-orbital injection. Blood was recovered by facial vein collection at days 1, 2, 3, 4, 5, 6, 7, 10, 14, 17, 22, 28, 35, 42 and 49 of the study. Serum samples were stored at $-20^{\circ}C$ until the end of the study when antibody concentrations were determined in parallel analysis using the Luminex anti-Spike binding assay with purified P5C3 and P5C3 LS used to generate standard binding curves.

QUANTIFICATION AND STATISTICAL ANALYSIS

All Luminex binding studies for Spike affinity and for detection of P5C3 antibody levels in plasma from hamsters and serum from hFcRn mice were performed with a 200 Bioplex instruments with data analysis and visualized using GraphPad Prism 8.3.0.

Cytopathic effect in the live virus neutralization assays was monitored by analyzing the density of live violet stained cells at a given concertation of antibody using ImageJ software (National Institutes of Health). Data analysis and figures were visualized using GraphPad Prism 8.3.0.

Luciferase signals detected for the SARS-CoV-2 Spike pseudoviral assays were measured on a Synergy H1 instrument (BioTek) using the Gen5 Software and with data analysis and visualized using GraphPad Prism 8.3.0.

Statistical parameters including the exact value of n, the definition of center, dispersion, and precision measures (Mean or Median ± SEM) and statistical significance are reported in the Figures and Figure Legends. Data were judged to be statistically significant when $p < 0.05$. In Figures, asterisks denote statistical significance as calculated using the two-tailed non- parametric Mann-Whitney U test for two groups' comparison. Analyses were performed in GraphPad Prism (GraphPad Software, Inc.) and Microsoft Excel. *In vivo* terminal half-lives for P5C5 and P5C3 LS were calculated using a one-phase exponential decay analysis.